Deanship of Graduate Studies
Al-Quds University

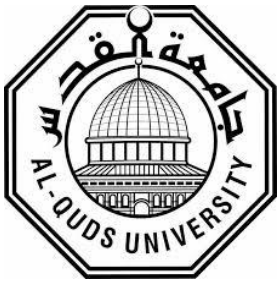

On Applying Partial Differential Equations in Image Processing

Sireen Waleed Ahmad Nasr

M. Sc. Thesis

Jerusalem - Palestine

1440/2019

On Applying Partial Differential Equations in Image Processing

Prepared by:
Sireen Waleed Ahmad Nasr

B. Sc: Bethlehem University, Palestine

Supervisor:
Dr: Yousef Hussein Zahaykah

A thesis submitted in partial fulfillment of requirements for the degree of Master of Mathematics, Department of Mathematics / Graduate Studies / Al - Quds University.

1440/2019

Al-Quds University

Deanship of Graduate Studies

Graduate Studies / Mathematics

Thesis Approval

On Applying Partial Differential Equations in Image Processing

Prepared by: Sireen Waleed Ahmad Nasr

Registration No: 21610003

Supervisor: Dr. Yousef Zahaykah

Master Thesis submitted and accepted, Date: 13/7/2019

The names and the signatures of the examining committee members are as follows:

1-Head of Committee	Dr.	Yousef Zahaykah	Signature: .....
2-Internal Examiner	Dr.	Jamil Jamal	Signature: .....
3-External Examiner	Dr.	Iyad Suwan	Signature: .....

Jerusalem – Palestine

1440/2019

Dedication

To my parents, my husband, my son, and to all those who supported me in completing this research.

Sireen Nasr

Declaration

I certify that this submitted for the degree of master is the result of my own research, except where otherwise acknowledge. And that this (or any part of the same) has not been submitted for a higher degree to any other university or institution.

Signed: .....

Sireen Waleed Ahmad Nasr

Date: 13/7/2019

Acknowledgment

Thanks is given first to God, for giving me the strength, knowledge, ability and opportunity to undertake this research. I am thankful to my supervisor Dr. Yousef Zahaykah for all his help and encouragement. Also, my thanks to t Al-Quds University for supporting this work, and I wish to pay my appreciation to all respected teachers and staff in the department of Mathematics.

Lastly, I offer my regards to all of those who supported me during the completion of this thesis.

Abstract

In this thesis we present a brief review of the assumed prerequisites in signals, linear time-invariant (LTI) systems and Fourier discrete-time systems with some of its properties. We derive the convolution formula, which allows us to determine the output of an LTI system to any given arbitrary input signal. Furthermore, we discuss the use of operators that can be used to remove noise and enhance signal, and we evolve the main principles for designing noise reduction and signal enhancement filters in the frequency and time domains. We introduce the design of notch and comb filters for removing periodic interference, enhancing periodic signals, and separating the luminance and chrominance components in digital color TV systems.

A major aim to the thesis is to use geometrical and variational partial differential equations (PSEs) in the process of image processing. We first derive and relate the p-Laplacians in terms of the concepts of gauge coordinates. We also present several PDE-based image denoising and enhancement models to evolve images, motivated by combining Gaussian blurring, the Mean Curvature Motion, for denoising and edge enhancement. We introducing the qualitative behavior by deriving a solution of the equations and mention its properties briefly. We also discuss the notions of curvature motion and edge affected diffusion filtering. Further in this thesis we implement and obtain quantitative and numerical results on a real-life image, showing the predictable behaviour on both noise-constrained and unconstrained evolution, one can vary the desired amount of blurring and denoising. At the end of the thesis the optimal homotopy asymptotic method (OHAM) is applied to derive a solution of the second order Gauge coordinate equation.

Contents

1 Introduction **2**
1.1 Digital Image 2
1.2 The Differential Structure of Images 7
1.3 Isophotes and Flow lines 11

2 Signal Processing **14**
2.1 Signals, Systems, and Signal Processing 14
2.2 Noise Reduction Filters 20
2.3 Digital Filters 24
2.4 TV and Video Comb Filters 30

3 Geometrical and Variational PDEs in Image Processing **43**
3.1 Using PDEs in Image Processing 44
3.2 Geometry Driven Scale-Space Filtering 54
3.3 Numerical Implementation 65
3.4 The optimal homotopy asymptotic Method (OHAM) 74

Appendix **82**

References **83**

Chapter 1

Introduction

1.1 Digital Image

Images are everywhere, since we rely on the images we see with our eyes more than any other tangible motivation. Almost all of the information we realize comes to us in the form of an image. In order to admire the theory and application of the image processing, we first need to understand the digital image. A digital image comes from a continuous one. We sampling and quantize analogue images to obtain such digital images. It is converted to a discretized form by a digitizer, which performs two tasks, known as sampling and quantization. Then the result is a digital image, and it can be used in digital image processing applications.

Example 1.1.1 *Fig. (1.1) shows sampling and quantization, in the sampling process, the values of the continuous signal are sampled at specific locations in the image. In the quantization process, the real values are discretized into digital numbers.*

A digital image is a matrix of real numbers. Each matrix element, i.e., a quantized sample, is called a picture element or a pixel, and its value is the gray-level or brightness, and it characterised by matrix size, pixel depth and resolution. The matrix size is determined from the number of the columns n and the number of rows m of the image matrix $m \times n$ as shown in Fig. (1.2). Generally, as the matrix dimension increases the resolution is getting better. Pixel or bit depth refers to the number of bits per pixel that represent the colour levels of each pixel in an image.

The term resolution of the image refers to the number of pixels per unit length of the image. In digital images the spatial resolution depends on pixel size. The pixel size is calculated by the Field of View (FoV) which is a measure of the ground area viewed by a single detector element in a given instant in time- divided by the

00	00	01	01	01	03	01	00
01	00	46	4a	45	7f	01	01
00	00	4a	5b	4c	63	00	01
00	04	4c	4c	4c	4c	4d	00
00	3d	4c	4c	4b	4c	49	00
00	0a	4d	4c	4d	4d	17	00
00	00	48	50	4d	57	01	00
00	00	01	02	10	00	01	01

Figure 1.1: Example of sampling and quantization. On the left an original image with continuous intensity values . On the middle a sampling using 8×8 locations, the image has real intensity values at specific locations only. And a quantization on the right (these real values are converted to discrete numbers)[17].

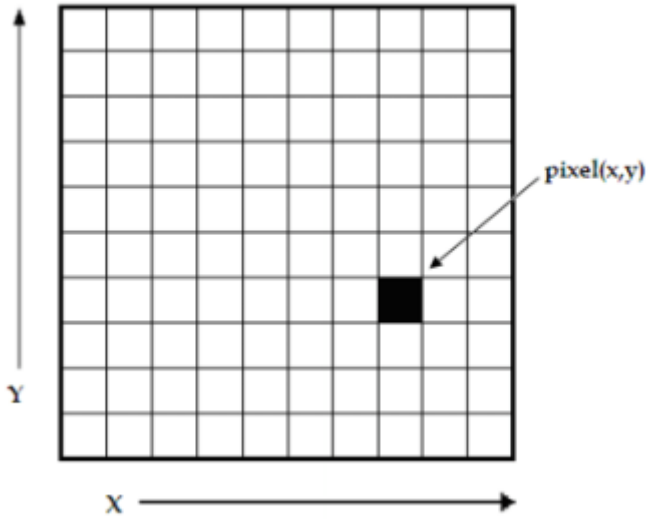

Figure 1.2: A digital image is a 2D array of pixels. Each pixel is characterised by its (x, y) coordinates and its value

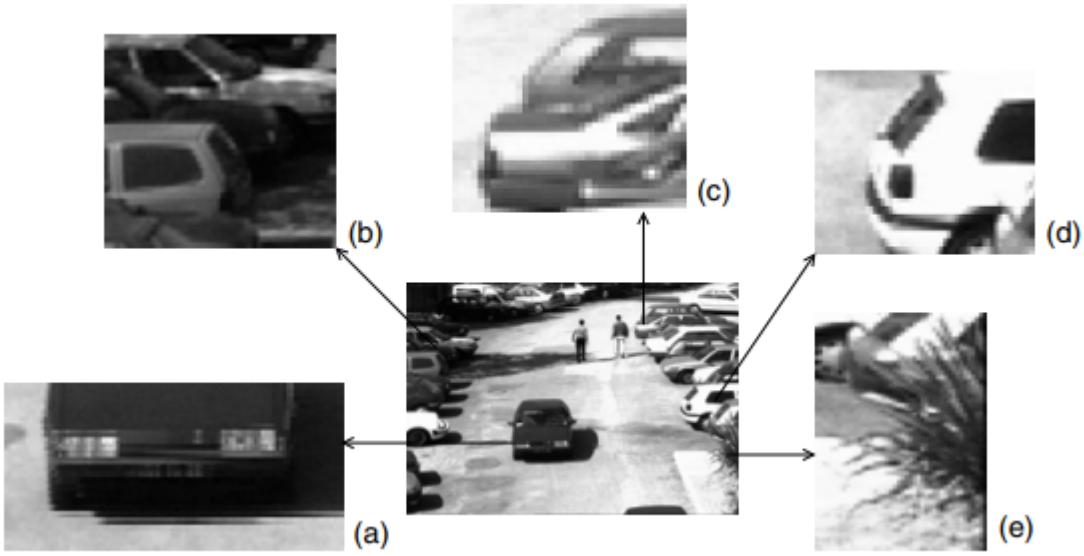

Figure 1.3: Different parts with different structures of the image [4]

number of pixels across the matrix. For a standard FoV, an increase of the matrix size decreases the pixel size and the ability to see details is improved. In a way, the higher the resolution, the closer the digital image is to the physical world.

To describe a pixel, one need several bands, as an example, a vector field has two components, a color image is described with three bands, red, green and blue. Another important characteristic concerning an image is the number of rows and the number of columns in that image, it is called the size of the image.

Example 1.1.2 *As in the real life, an image is composed of a wide variety of structures, and this is even more complex because of the digitalization and the limited number of gray levels to represent it, see [4].To have a better look, an image and some close-ups on different parts are shown in Fig. (1.3).*

The standard slot shape in todays photographic equipments is square, as it is easy to fabricate on a detector chip. The effect appears clearly when we zoom in to pixel level.

Example 1.1.3 *The face in Fig.* (1.4) *certainly has no square corners all over and sharp edge discontinuities. So what is the shape of the optimal aperture?*

The derivation of the optimal shape can be based on the measurements taken

Figure 1.4: Typically pixels are measured with the wrong aperture function, such as squares. Sharp edges and corners that are not in the original scene [8].

by a finite aperture, all locations are treated similarly, (this leads to translation invariance), and the using of the superposition principle (the measurement should be linear). see [8].

By these principles the observation must be a convolution, for simplicity consider the 1D convolution example :

$$h(x) = \int_{-\infty}^{\infty} L(y)g(x-y)dy,$$

where $L(x)$ is the luminance, $g(x)$ is the unknown aperture (positive function) and $h(x)$ the result of the measurement.

Definition 1.1.1 *The entropy H of the filter is defined as*

$$H = \int_{-\infty}^{\infty} -g(x)log(g(x))dx$$

It measures the spurious extras (the maximal disorder) when filter is used.

We need to determine the $g(x)$, for which the entropy is minimal given the constraints:

$$\int_{-\infty}^{\infty} g(x)dx = 1, \qquad \text{(normalization constraint)},$$

$$\int_{-\infty}^{\infty} xg(x)dx = 0, \qquad \text{(first moment of } g(x)),$$

and

$$\int_{-\infty}^{\infty} x^2 g(x)dx = \sigma^2 \qquad \text{(second moment of } g(x)).$$

Applying Lagrange multipliers method, The entropy under the given constraints reads

$$\tilde{H} = \int_{-\infty}^{\infty} -g(x)log(g(x))dx + \lambda_1 \int_{-\infty}^{\infty} g(x)dx + \lambda_2 \int_{-\infty}^{\infty} xg(x)dx + \lambda_3 \int_{-\infty}^{\infty} x^2 g(x)dx$$

where λ_1, λ_2, and λ_3 are scalars (Lagrange multipliers). According to this method $\tilde{H}$ (minimal) when $\dfrac{\partial \tilde{H}}{\partial g} = 0$. This gives

$$\frac{\partial H}{\partial g} = \int_{-\infty}^{\infty} -1 - log[g(x)]dx + \int_{-\infty}^{\infty} \lambda_1 dx + \int_{-\infty}^{\infty} \lambda_2 x dx + \int_{-\infty}^{\infty} \lambda_3 x^2 dx = 0,$$

$$-1 - log[g(x)] + \lambda_1 + x\lambda_2 + x^2\lambda_3 = 0$$

or the last equations leads to

$$g(x) = e^{-1+\lambda_1+x\lambda_2+x^2\lambda_3} \tag{1.1}$$

The scalar λ_3 must be less than zero, otherwise the function $g(x)$ explodes as x approaches infinity, which is physically irrelevant. By substituting from (1.1) into the three constaints and noting that λ_3 is negative we get respectively

$$e\sqrt{-\lambda_3} = e^{\lambda_1 - \frac{\lambda_2^2}{4\lambda_3}}\sqrt{\pi},$$

$$e^{\lambda_1 - \frac{\lambda_2^2}{4\lambda_3}}\lambda_2 = 0,$$

$$\text{and} \quad \frac{\mathrm{e}^{-1+\lambda_1 - \frac{\lambda_2^2}{4\lambda_3}}\sqrt{\pi}(\lambda_2^2 - 2\lambda_3)}{4(-\lambda_3)^{5/2}} = \sigma^2.$$

Solving the three equations for λ_1, λ_2 and λ_3 gives

$$\lambda_1 = \frac{1}{4} log\left[\frac{e^4}{4\pi^2\sigma^4}\right],$$

$$\lambda_2 = 0,$$

$$\lambda_3 = -\frac{1}{2\sigma^2 e},$$

clearly λ_3 is negative. Using Eq.(1.1) the aperture function $g(x)$ reads

$$g(x) = \frac{1}{\sqrt{2\pi}\sigma} e^{-\frac{x^2}{2\sigma^2}}$$

which is the Gaussian kernel.

It is important to note that the Gaussian kernel is the only solution of the previous constaints. Further, it is circular and generates no suprious resolution, being very smooth.

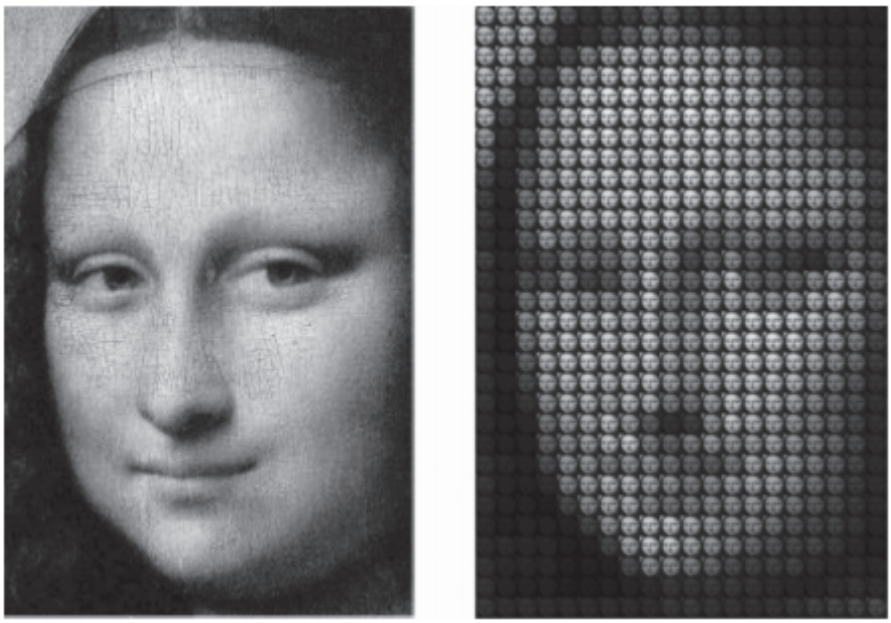

Figure 1.5: Mona Lisa at different scales [8].

Example 1.1.4 *Fig.* (1.5) *shows Mona Lisa at different scales, the Gaussian kernel blurs the image, but that is the natural consequence of an observation with a finite aperture. We cannot see molecules with our naked eye, [8].*

1.2 The Differential Structure of Images

Details of images exist only over a restricted range of scale. Hence it is important to study the image structure, which can be described as the local multi-scale derivatives of the image, using heightlines, local coordinate systems and independence of the choice of coordinates. We will also use the tools of differential geometry, which is defined as the framework of finite-dimensional real manifolds, employing methods from analysis to investigate geometric problems, involving the shape of smooth curves and surfaces, lines, spaces, surfaces etc.

An important property of real-world images is that they are exist as significative structure over definite ranges of scale. For example, the notion of a section of a tree, which makes sense only at a scale from, say, a few centimeters to at most a few meters. It is meaningless to discuss the tree notion at the nanometer or kilometer level. At those scales, it is more relevant to talk about the molecules that form the leaves of the tree, and the forest in which the tree grows, respectively. This fact, that images are shown in different ways according on the scale of

observation, has important implications if one aims at describing them. It shows that the notion of scale is of utmost importance.

Scale-space theory provides a mathematically convenient method to generate representations of images at multiple scales, which also handle the above-mentioned multi-scale nature of image data. The reasoning behind its construction is that if no prior information is available about what are the appropriate scales for a given data set, then the only reasonable approach for an uncommitted vision system is to represent the input data at multiple scales.

Example 1.2.1 *Take a look at Fig.* (1.6). *This painting contains a wealth of objects "living" at a wide range of scales, from small-scale objects such as the cracks in the pavement to large-scale structures such as the building in the background.*

An essential requirement is that structures at coarse scales in the multi−scale representation should frame simplifications of corresponding structures at finer scales−they should not be occasional phenomena formed by the method for repress fine-scale structures. This idea has been formalized in a different ways by different Researchers. A noteworthy coincidence is that similar results can be observed from several different points. A main result is that if rather general conditions are imposed on the types of computations that are to be performed, then convolution by the Gaussian kernel and its derivatives is singled out as a canonical class of smoothing transformations. The requirements (scale−space axioms) that specify the uniqueness are essentially linearity and spatial shift invariance, combined with different ways of formalizing the notion that new structures hould not be created in the transformation from fine to coarse scales, [15].

In summary, for any N-dimensional signal $f : R^N \longrightarrow R$, its scale-space representation $L : R^N \times R_+ \longrightarrow R$ is defined by

$$L(x;t) = \int_{\xi \in R^N} f(x-\xi) g(\xi, t) d\xi$$

where $g : R^N \times \mathbb{R}_+ \longrightarrow \mathbb{R}_+$ denotes the Gaussian kernel.

$$g(x;t) = \frac{1}{(2\pi t^2)^{N/2}} e^{-(x_1^2 + \ldots + x_N^2)/2t}$$

and the variance t of this kernel is referred to as the scale parameter. And the scale space can be viewed as a stack of images, where the original image is at the bottom of the stack $f_0(x, y) = f(x, y)$, and the image resolution gets lower as we rise in the stack, see Fig. (1.7).

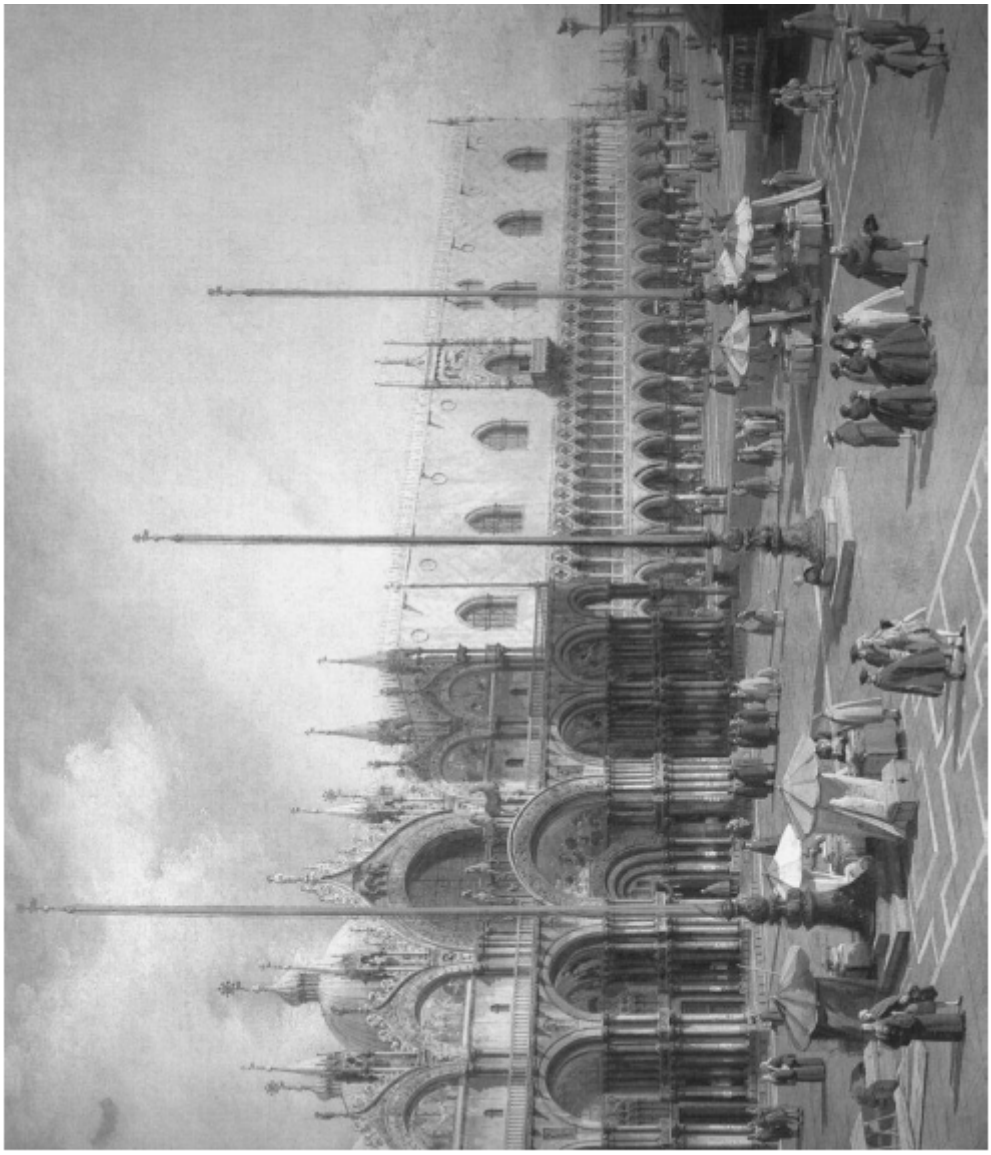

Figure 1.6: Canaletto′s San Marco square. An example of a scene with objects at multiple scales [17].

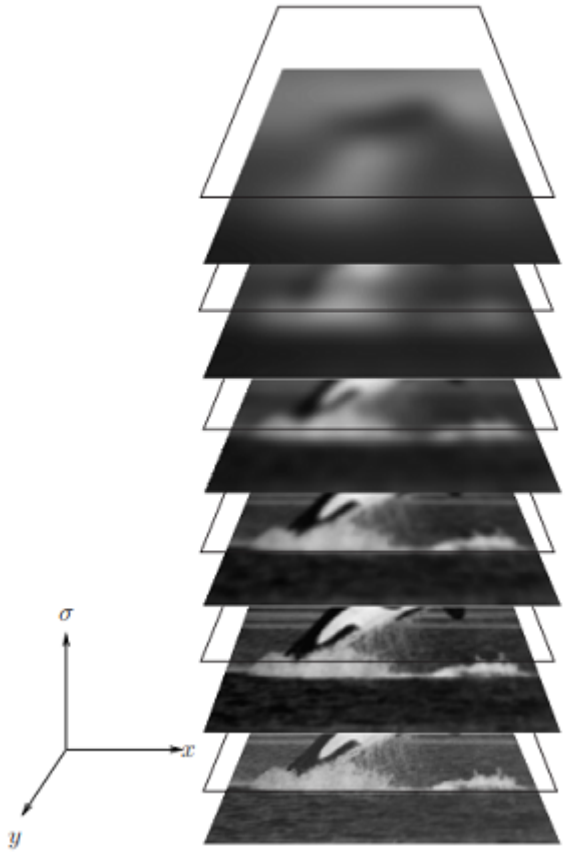

Figure 1.7: The scale space of an image. The original image rests at the bottom of the stack ($\sigma = 0$), and the scale σ increases as we rise in the stack [17].

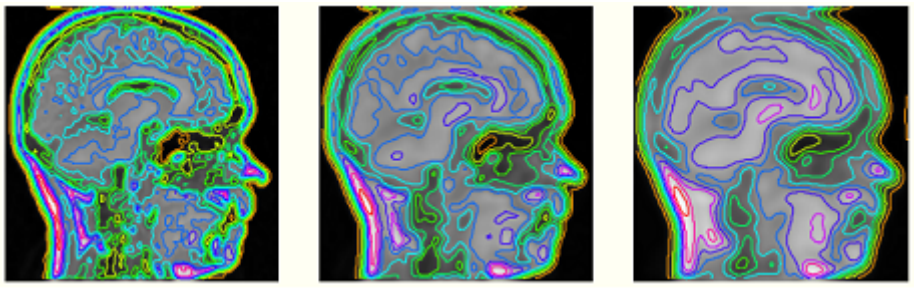

Figure 1.8: Isophotes at different scales, several isophotes are plotted in each image over the available intensity range. Each is appear in a different color [23].

1.3 Isophotes and Flow lines

The most natural set of contours that describe an image are its isophotes, which can be defined as lines in the image connecting points of equal intensity. They are also the heightlines if the image viewed as a landscape, when we consider the intensity as 'height'. The complete set of isophotes fully describes an image .The image isophotes can also be defined in a much more intuitive way: they are the curves of constant grey value $L(x, y) = c$,

Example 1.3.1 *Fig. (1.8) shows isophotes of an image at various bluring scales. Ten isophtes are plotted in each image, equldistant over the available intensity range. Each is shown in a different color, superimposed over the grayvalues. Notice that the isophotes get more rounded when we blure the image. When we consider the intensity distibution of a* $2D$ *image as a landscape, where the height is given by the intensity, isophotes are the heightlines.*

Isophotes are important elements of an image. In fact, all isophotes in the image contain the same information as the image. The known and often surprisingly good working segmentation method by thresholding which used to segment an image by setting all pixels whose intensity values are above a threshold luminance is an example of an important application of isophotes.

Isophotes have the following properties [23]:

1. Isophotes are closed curves. Most isophotes in 2D images are a so-called Jordan curve: a non-self-intersecting planar curve topologically equivalent to a circle;

2. Isophotes can intersect themselves. These are the critical isophotes. These always go through a saddle point.

3. Isophotes do not intersect other isophotes.

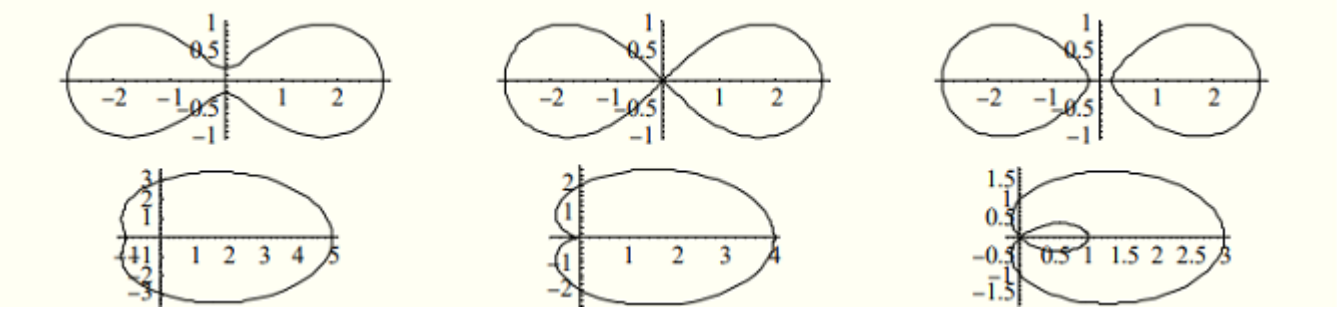

Figure 1.9: Top row: Split and join of an isophote . Bottom row: Self intersection of an isophote [23].

4. Any planar curve is completely described by its isophotes.

5. Isophote shape is independent of grayscale transformations, such as changing the contrast or brightness of an image.

A particular case of isophotes is created by those isophotes that go through a singularity in the intensity landscape, thus through a minimum, maximum or saddle point. The intensity landscape is horizontal at these places.

Example 1.3.2 *Isophotes intersect themselves at saddle points which make the above and the beneath of this intersection a different neighbor isophotes, they have divide from one curve into two, or joint from two curves into one see Fig. (1.9).*

At a minimum or maximum the isophote has shrunk to a point, and going to higher or lower intensity gives rise to the creation or vanishing of isophotes.

Example 1.3.3 *Fig. (1.10) shows an example of an image where only three Gaussian 'blobs' are present. The saddle points are in between the blobs. Isophotes through saddles and extrema are called critical isophotes.*

The isophotes have a natural dual, the flow lines (also known as slope lines or maximum gradient paths). These are the paths of the gradient and so intersect the isophotes orthogonally. They are familiar in ordinary life as the paths of water droplets flowing downhill (equating luminance with height). Flowlines are everywhere and they are perpendicular to the isophotes.

Flow lines are the integral curves of the gradient, made up of all the small little gradient vectors in each point integrated to a smooth long curve.

Example 1.3.4 *In 2D, the flowlines and the isophotes together form a mesh or grid on the intensity surface. The complete set of flowlines fully describes an image. It also have a singularity at minima and maxima just like the isophote, see Fig. (1.11).*

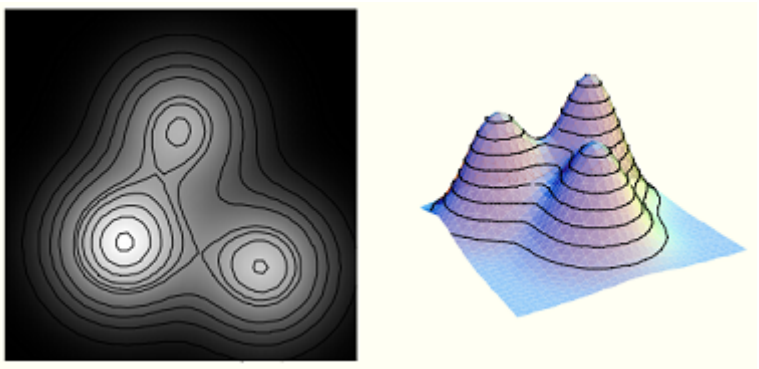

Figure 1.10: Isophote on a 2D 'landscape' , shown as heightlines [23].

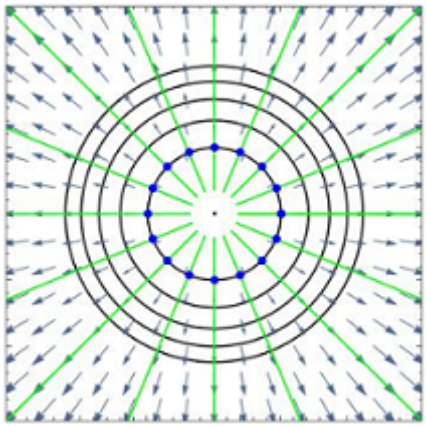

Figure 1.11: Isophotes and flow lines . The circles are the isophotes, the flow lines are everywhere perpendicular

Chapter 2

Signal Processing

The signal processing operations involved in many applications like communication systems, control systems, instrumentation, biomedical signal processing etc can be implemented in two different ways. Analog or continuous time method and digital or discrete time method. Any information generated in the signal processing is a signal. It could be an image, an analog voice signal or a digital signal of processor etc. The extraction of information from complex signals in the presence of noise, generally by conversion of the signals or appling various processing algorithms to enhance signal quality or encodining the information for security purposes and alot other, all these things come under the name signal processing.

In this chapter the characterization of discrete-time systems Fourier transform in general, and a number of its proprties are defined. We introduce the linear time-invariant (LTI) systems, and derived an important formula, called the convolution formula, that allows us to determine the output of an LTI system to any given arbitrary input signal. Moreover, we present some details about noise reduction and signal enhancement, which is one of the main applications of the signal prcessing and is of importance to engineers and scientists who extract noise from data. Here, we evolve the main principles for designing noise reduction and signal enhancement filters in the frequency and time domains. We introduce the design of notch and comb filters for removing periodic interference, enhancing periodic signals, and separating the luminance and chrominance components in digital color TV systems.

2.1 Signals, Systems, and Signal Processing

A signal is defined as any physical quantity that varies with time, space, or any other independent variable or variables. Mathematically, we describe a signal as

a function of one or more independent variables. A system may also be defined as a physical device that performs an operation on a signal. For example, a filter used to reduce the noise and interference corrupt in desired information bearing signal is called a system. In this case the filter performs some operations on the signal, which has the effect of reducing (filtering) the noise and interference from the desired information bearing signal.

When we pass a signal through a system, as in filtering, we say that we have processed the signal. In this case the processing of the signal involves filtering the noise and interference from the desired signal. In general, the system is characterized by the type of operation that it performs on the signal. For example, if the operation is linear, the system is called linear. If the operation on the signal is nonlinear, the system is said to be nonlinear. Such operations are usually referred to as signal processing.

The Discrete Time Fourier Transform

The Fourier representation of signals plays an important role in both continuous and discrete signal processing. The discrete time Fourier transform can be found by taking the continuous time Fourier transform of a sampled signal [21, 22].

The discrete-time Fourier transform (DTFT) or The frequency spectrum of a sampled signal $x(n)$ is defined as follows:

$$X(\omega) = \sum_{n=-\infty}^{\infty} x(n)e^{-j\omega n} \tag{2.1}$$

In order for the DTFT, Eq.(2.1), of a sequence to exist, the summation must converge. It will hold if $x(n)$ is absolutely summable, that is if

$$\sum_{n=-\infty}^{\infty} |x(n)| < \infty.$$

Note that the DTFT of a discrete-time sequence is a function of a continuous variable ω.

The DTFT is periodic in ω with a period of 2π, to show this fact notice that

$$\begin{aligned} X(\omega + 2\pi) &= \sum_{n=-\infty}^{\infty} x(n) e^{-jn(\omega+2\pi)} \\ &= \sum_{n=-\infty}^{\infty} x(n) e^{-jn\omega} e^{-jn2\pi} \\ &= \sum_{n=-\infty}^{\infty} x(n) e^{-jn\omega} = X(\omega). \end{aligned}$$

Since the DTFT is periodic in ω with a period of 2π, we can express it by an exponential Fourier series as follows:

$$X(\omega) = \sum_{n=-\infty}^{\infty} c_n e^{j\omega n} = \sum_{n=-\infty}^{\infty} c_{-n} e^{-j\omega n} \tag{2.2}$$

where

$$c_{-n} = \frac{1}{2\pi} \int_{-\pi}^{\pi} X(\omega) e^{jn\omega} d\omega.$$

Comparing equations (2.1) and (2.2) shows that the discrete signal $x(n)$ corresponds to the spectrum $X(\omega)$, that is $x(n) = c_{-n}$.

The inverse discrete-time Fourier transform is given by

$$x(n) = \frac{1}{2\pi} \int_{-\pi}^{\pi} X(\omega) e^{jn\omega} d\omega. \tag{2.3}$$

The proof of this claim goes as follows:

$$\begin{aligned} \frac{1}{2\pi} \int_{-\pi}^{\pi} X(\omega) e^{jn\omega} d\omega &= \frac{1}{2\pi} \int_{-\pi}^{\pi} \left(\sum_{m=-\infty}^{\infty} x(m) e^{-jm\omega} \right) e^{jn\omega} d\omega \\ &= \frac{1}{2\pi} \sum_{m=-\infty}^{\infty} x(m) \int_{-\pi}^{\pi} e^{j(n-m)\omega} d\omega. \end{aligned}$$

Because the integral on the right-hand side vanishes except when $m = n$, the equation can be simplified as

$$\begin{aligned} \frac{1}{2\pi} \int_{-\pi}^{\pi} X(\omega) e^{jn\omega} d\omega &= \frac{1}{2\pi} x(n) \int_{-\pi}^{\pi} e^{j\cdot 0\omega} d\omega \\ &= \frac{1}{2\pi} x(n) \cdot 2\pi \\ &= x(n). \end{aligned}$$

Theorem 2.1.1 (Shift in time) *Let $y(n)$ be the delay of $x(n)$ by m samples, i.e.*

$$y(n) = x(n-m)$$

for all n. Then

$$Y(\omega) = e^{-jm\omega} \cdot X(\omega).$$

proof

$$\begin{aligned} Y(\omega) &= \sum_{n=-\infty}^{\infty} x(n-m)e^{-j\omega n} \\ &= \sum_{k=-\infty}^{\infty} x(k)e^{-j\omega(m+k)} \\ &= e^{-j\omega m} \sum_{k=-\infty}^{\infty} x(k)e^{-j\omega k} \\ &= X(\omega)e^{-j\omega m} \end{aligned}$$

Theorem 2.1.2 (Linearity) *The DTFT is a linear operator. This means if the DTFT of $x(n)$ and $y(n)$ are $X(\omega)$ and $Y(\omega)$ respectively and if α and β are scalars then the DTFT of $\alpha x(n) + \beta y(n)$ is $\alpha X(\omega) + \beta Y(\omega)$*

proof

$$\begin{aligned} DTFT &= \sum_{n=-\infty}^{\infty} \left(\alpha x(n) + \beta y(n)\right) e^{-j\omega n} \\ &= \sum_{n=-\infty}^{\infty} \left(\alpha x(n)e^{-j\omega n} + \beta y(n)te^{-j\omega n}\right) \\ &= \alpha \sum_{n=-\infty}^{\infty} x(n)e^{-j\omega n} + \beta \sum_{n=-\infty}^{\infty} y(n)e^{-j\omega n} \\ &= \alpha X(\omega) + \beta Y(\omega). \end{aligned}$$

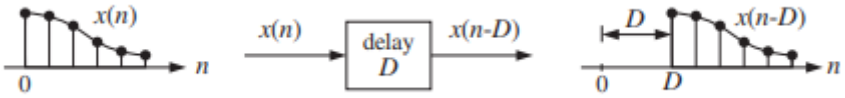

Figure 2.1: Time delay by D samples.

Time-Invariant Systems

A time-invariant system is a system that remains unchanged over time, [18]. This implies that if an input is applied to the system today causing a certain output to be produced, then the same output will also be produced tomorrow if the same input is applied.

Example 2.1.1 *The operation of waiting or delaying a signal by a time delay of, say, D units of time is shown in Fig. (2.1). It represents the right translation of $x(n)$ as a whole by D samples. A time advance would have negative D and correspond to the left translation of $x(n)$.*

We note that a system is a linear time-invariant (LTI) if the relation between its input and output satisfies Linearity and time-invariance because if a stimulus $x_1(n)$, $n = 0, 1, 2, \cdots$ causes response $y_1(n)$, and $x_2(n)$ causes $y_2(n)$, then $ax_1(n) + bx_2(n)$ causes $ay_1(n) + by_2(n)$. And if $x(n)$, $n = 0, 1, 2, \cdots$ causes a response $y(n)$, then $x(n - m)$, where m is a fixed integer, causes $y(n - m)$.

Remark 2.1.1 *An LTI system is characterized by its impulse response $h(n)$ in the sense that, given any arbitrary input $x(n)$, then the output $y(n)$ can be calculated according to the convolution of $x(n)$ and $h(n)$*

$$y(n) = x(n) * h(n) = \sum_{m=-\infty}^{n} x(m) \cdot h(n - m)$$

The convolution theorem

The convolution in the time domain corresponds to multiplication in the frequency domain. Conceptually, if we take a signal as the input to an LTI system and the other signal as the impulse response of the LTI system. Then, we can calculate the output spectrum by multiplying the input spectrum with the transfer function of the LTI system.

Theorem 2.1.3 *Let $x_1(n)$ and $x_2(n)$ be two discrete-time signals. If*

$$y(n) = x_1(n) * x_2(n)$$

then

$$Y(\omega) = X_1(\omega) \cdot X_2(\omega).$$

Proof

$$\begin{aligned} Y(\omega) &= \sum_{n=-\infty}^{\infty} y(n) e^{-j\omega n} \\ &= \sum_{n=-\infty}^{\infty} \left(\sum_{m=-\infty}^{\infty} x_1(m) \cdot x_2(n-m) \right) e^{-j\omega n} \\ &= \sum_{m=-\infty}^{\infty} x_1(m) \left(\sum_{n=-\infty}^{\infty} x_2(n-m) e^{-j\omega n} \right). \end{aligned}$$

Let $k = n - m$ then $n = m + k$ and we get

$$\begin{aligned} Y(\omega) &= \sum_{m=-\infty}^{\infty} x_1(m) \left(X_2(\omega) e^{-j\omega m} \right) \\ &= X_2(\omega) \sum_{m=-\infty}^{\infty} x_1(m) e^{-j\omega m} \\ &= X_2(\omega) X_1(\omega). \end{aligned}$$

Theorem 2.1.4 (Parseval's) *Let $x(n)$ be a real-valued, discrete-time signal and $X(\omega)$ be its DTFT Then, the following equation always holds:*

$$\sum_{n=-\infty}^{\infty} x^2(n) = \frac{1}{2\pi} \int_{-\pi}^{\pi} |X(\omega)|^2 d\omega$$

Proof
Consider the autocorrelation function

$$y(m) = \sum_{n=-\infty}^{\infty} x(n) x(n-m)$$

Note that $y(n) = x(n) * x(-n)$, and $y(0) = \sum_{n=-\infty}^{\infty} x^2(n)$. By applying the convolution theorem, $y(n)$'s Fourier transform of $Y(\omega)$ can be expressed in terms

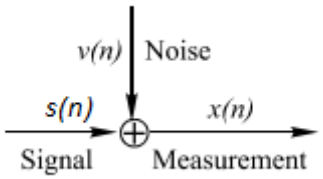

Figure 2.2: Measurements of a signal with noise,

of $X(\omega)$ as follows

$$Y(\omega) = X(\omega) \cdot \left(\sum_{n=-\infty}^{\infty} x(-n) e^{-j\omega n} \right) = X(\omega) \cdot X^*(\omega) = |X(\omega)|^2.$$

Using the inverse DTFT at time 0 we get

$$\sum_{n=-\infty}^{\infty} x^2(n) = y(0) = \frac{1}{2\pi} \int_{-\pi}^{\pi} Y(\omega) e^{j\omega \cdot 0} d\omega$$

$$= \frac{1}{2\pi} \int_{-\pi}^{\pi} |X(\omega)|^2 d\omega.$$

2.2 Noise Reduction Filters

Much of signal processing involves extracting signals of interest from noise. A filter is a system that is designed to process signals into those we desire. The purpose of using a filter can be various, to extract a desired signal from noisy data (measurement), to transform signals, to suppress noise, to separate two signals that are mixed in one measurement, etc. Consider a signal $s(n)$,

$$x(n) = s(n) + v(n) \tag{2.4}$$

where $v(n)$ is the undesired noise component, illustrated in Fig. (2.2).

In signal processing to extract a desired signal $s(n)$, from $x(n)$ we design an appropriate filter $H(z)$ which clears the noise component $v(n)$ and at the same time keeps the desired signal $s(n)$ unchanged. Using linearity, we can express the output signal in the form:

$$y(n) = y_s(n) + y_v(n)$$

where $y_s(n)$ is the output corresponds to the signal $s(n)$ and $y_v(n)$ the output corresponds to the noise signal $v(n)$.
For the filter we require $y_v(n)$ be vary small as we can and $y_s(n)$ be as similar to $s(n)$ as possible; namely we need

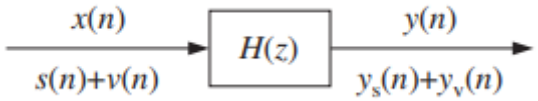

$$y_s(n) = s(n)$$
$$y_v(n) = 0$$

To determine when these conditions are satisfied, we express them in the frequency domain in terms of the corresponding frequency spectra as follows:$Y_s(\omega) = S(\omega)$ and $Y_v(\omega) = 0$. Applying the filtering equation $Y(\omega) = H(\omega)X(\omega)$ separately to the signal and noise components, we have the conditions, [19]:

$$Ys(\omega) = H(\omega)S(\omega) = S(\omega) \tag{2.5}$$

$$Y_v(\omega) = H(\omega)V(\omega) = 0 \tag{2.6}$$

In general, conditions (2.5) and (2.6) cannot be satisfied simultaneously. Since condition (2.5) requires $H(\omega) = 1$ for all ω, for which the signal spectrum is nonzero, $S(\omega) \neq 0$. While condition (2.6) requires $H(\omega) = 0$ for all ω, for which the noise spectrum is nonzero, $V(\omega) \neq 0$. These two conditions can be satisfied at same time only if the signal and the noise spectra do not intersect.

Example 2.2.1 *In Fig. (2.3), the filter $H(\omega)$ have passband that coincides with the signal band, and stopband that coincides with the noise band. The filter keep the signal spectrum unchanged by only removing the noise spectrum. But, if the signal and noise spectra overlap, as usual, then the previous conditions cannot be satisfied simultaneously, because there would be values of ω such that both $S(\omega) \neq 0$ and $V(\omega) \neq 0$ and therefore the conditions would require $H(\omega) = 1$ and $H(\omega) = 0$ for the same ω.*

Noise Reduction Rating

A Noise Reduction Rating or NRR is a system used to measure the amount a hearing protection device is capable of reducing sound exposure in decibels. The higher the NRR of a hearing protector, the more effective it will be at reducing noise.

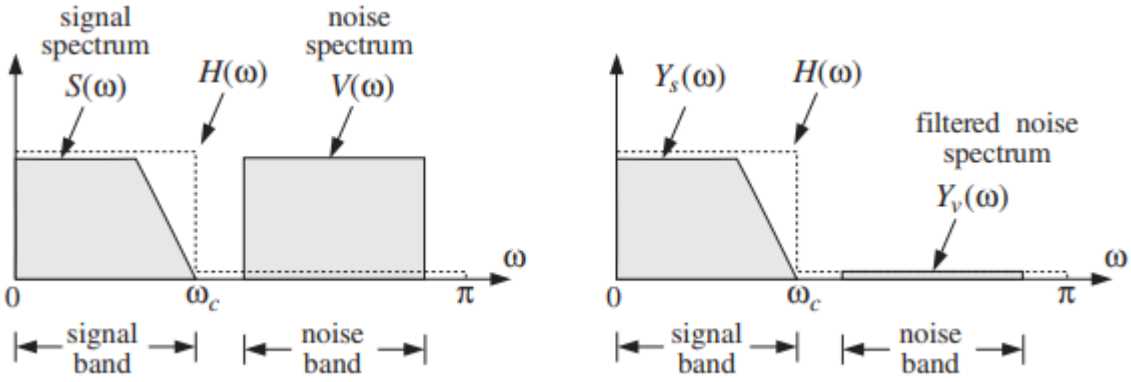

Figure 2.3: Signal and noise spectra before and after filtering [19].

Definition 2.2.1 *The autocorrelation function is a function that defined as a correlation between $x(n)$ and $x(n+k)$, which separated by a time lag k:*

$$R_{xx}(k) = E[x(n+k)x(n)].$$

Definition 2.2.2 *The power spectrum represents the frequency content of the random signal $x(n)$, it is defined as the discrete-time Fourier transform of its autocorrelation function $R_{xx}(k)$.*

$$S_{xx}(\omega) = \sum_{k=-\infty}^{\infty} R_{xx}(k)e^{-j\omega k},$$

where $\omega = 2\pi f/f_s$ is the digital frequency in radians per sample.

Using the inverse DTFT to expresses $R_{xx}(k)$ in terms of $S_{xx}(\omega)$ we have

$$R_{xx}(k) = E[x(n+k)x(n)] = \int_{-\pi}^{\pi} S_{xx}(\omega)e^{j\omega k}\frac{d\omega}{2\pi}.$$

Theorem 2.2.1 *Let x(n) be a signal, to get the variance, or the average power, of the signal $x(n)$, we set $k = 0$. Then we obtain*

$$\sigma_x^2 = R_{xx}(0) = E[x(n)^2] = \int_{-\pi}^{\pi} S_{xx}(\omega)\frac{d\omega}{2\pi} = \int_{\frac{-fs}{2}}^{\frac{fs}{2}} S_{xx}(f)\frac{df}{f_s} \tag{2.7}$$

where

$$S_{xx}(f) = \sum_{k=-\infty}^{\infty} R_{xx}(k)e^{-2\pi jfk/f_s}.$$

Remark 2.2.1

1. *The quantity* $\frac{S_{xx}(f)}{f_s}$ *represents the power per unit frequency interval.*
2. *The power spectrum or spectral density Eq. (2.7) describes the distribution of power into frequency components composing that signal. Its integral over the Nyquist interval, Eq. (2.7) , gives the total power in the signal.*

Proposition 2.2.1 *Usually more convenient to use the z-transform of the auto-correlation and replace* $z = e^{j\omega} = e^{2\pi jf/f_s}$ *to obtain the power spectrum* $S_{xx}(\omega)$ *or* $S_{xx}(f)$ *:*

$$S_{xx}(z) = \sum_{k=-\infty}^{\infty} R_{xx}(k)z^{-k}.$$

Proposition 2.2.2 *The relation between input spectral density and output spectral density is*

$$S_{yy}(\omega) = |H(\omega)|^2 S_{xx}(\omega).$$

Proposition 2.2.3 *The input spectrum is reshaped by the filter spectrum. The filtering equation in the frequency domain is* $Y(\omega) = H(\omega)X(\omega)$*, and in the z-domain is* $Y(z) = H(z)X(z)$*. Using the special case of a white noise input with a flat spectral density* $S_{xx}(\omega) = \sigma_x^2$*, the output periodogram will be related to the input periodogram as follows:*

$$S_{yy}(\omega) = |H(\omega)|^2 \sigma_x^2.$$

Proposition 2.2.4 *A measure of whether the filter attenuates or magnifies the input noise is given by the variance of the output* σ_y^2*. Applying Eq. (2.7)*

$$\sigma_x^2 = R_{xx}(0) = E[x(n)^2] = \int_{-\pi}^{\pi} S_{xx}(\omega)\frac{d\omega}{2\pi} = \int_{\frac{-f_s}{2}}^{\frac{f_s}{2}} S_{xx}(f)\frac{df}{f_s}$$

to $y(n)$, we get:

$$\sigma_y^2 = \int_{-\pi}^{\pi} S_{yy}(\omega)\frac{d\omega}{2\pi} = \sigma_x^2 \int_{-\pi}^{\pi} |H(\omega)|^2 \frac{d\omega}{2\pi}.$$

Using Parseval′s equation, which relates the total energy of a sequence to its spectrum,

$$\sum_{n=-\infty}^{\infty} |x(n)|^2 = \frac{1}{2\pi}\int_{-\pi}^{\pi} |X(\omega)|^2 d\omega,$$

we can write NRR in the form:

$$NRR = \frac{\sigma_y^2}{\sigma_x^2} = \int_{-\pi}^{\pi} |H(\omega)|^2 \frac{d\omega}{2\pi} = \sum_n h(n)^2 \tag{2.8}$$

Signal-to-noise ratio

The signal-to-noise ratio (SNR), defined as the ratio of the signal variance to the variance of the system noise, or in decibels as $10\log_{10}(SNR)$, is a broadly accepted measure for characterizing system fidelity and for comparing performance characteristics between different systems .The higher the ratio, the less distorted the signal is by the noise.

Definition 2.2.3 *The SNRs at the input and output of the filter are defined as*

$$SNR_{in} = \frac{\sigma_s^2}{\sigma_v^2}, \quad SNR_{out} = \frac{\sigma_{ys}^2}{\sigma_{yv}^2}.$$

Therefore,

$$\frac{SNR_{out}}{SNR_{in}} = \frac{\sigma_{ys}^2}{\sigma_{yv}^2} \cdot \frac{\sigma_v^2}{\sigma_s^2} = \frac{1}{NRR} \cdot \frac{\sigma_{ys}^2}{\sigma_s^2}.$$

If the desired signal is not changed by the filter, $y_s(n) = s(n)$, then

$$\frac{SNR_{out}}{SNR_{in}} = \frac{1}{NRR}.$$

Thus, maximizing the signal−to noise ratio is equivalent to minimizing the noise reduction ratio at the filter′s output.

2.3 Digital Filters

The term filter is commonly used to describe a device that discriminates, according to some distribute of the object applied at the input, what passes through it, e.g., an air filter that allows air to pass through it but prevents dust particular that are present in the air from passing through. An oil filter performs a similar function, with the exception that oil is a substance allowed to pass through the filter, while particles of dirt are collected at the input of filter and prevented from passing through it.

So the filter is used in digital signal processing in a variety of ways, such as removal

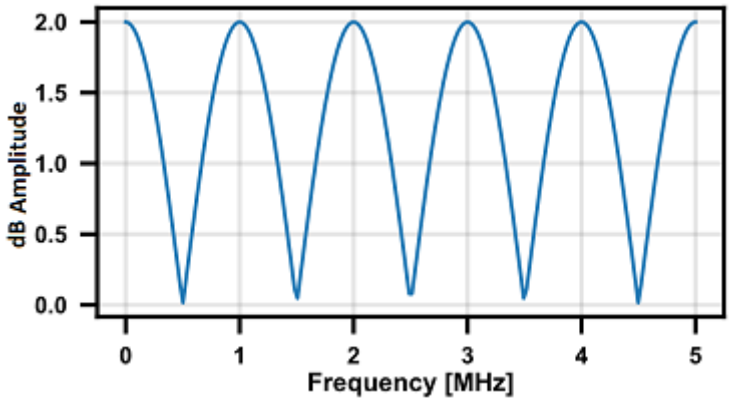

Figure 2.4: Comb filter.

of undesirable noise from desired signal, spectral shaping such as equalization of communication channels, signal detection in radar, sonar and communication and for performing spectral of signal.

Comb Filters

Filters are analog circuits which performs signal processing function. It is used to specially remove unwanted frequency components from the signal to enhance wanted ones. A comb filter is a Linear Time-Invariant (LTI) digital filter, implemented by adding a delayed version of a signal to itself, causing constructive and destructive interference. Comb filters are used in a number of signal processing application such as television decoders, and audio effects.

Example 2.3.1 *Fig. (2.4) shows a comb filter, the frequency response of a comb filter consists of a series of regularly spaced notches, The name comb is derived by the fact that its magnitude response resembles the teeth of a comb, as shown in Fig. (2.4). Since there are several filters having magnitude responses with such characteristic, the term comb filter is rather general.*

The duration of the impulse response of comb filters can be either finite or infinite, i.e., there are Finite Impulse Response (FIR) comb filters and Infinite Impulse Response (IIR) comb filters.

The Finite Impulse Response (FIR) comb filter adds a delayed version of the input signal to itself as shown in Fig. (2.5) and is represented by the equation, [10]:

$$y(n) = x(n) + \alpha x(n - k)$$

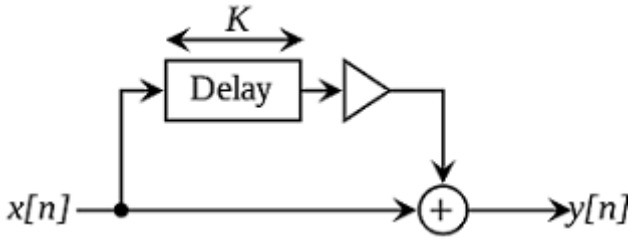

Figure 2.5: FIR comb filter structure [10].

and the impulse response of this filter is :

$$h(n) = \delta(n) + \alpha\delta(n-k)$$

where k is the delay length (measured in samples),[27], and α is a scaling factor applied to the delayed signal. If we use the z transform which is defined as the formal power series $X(z)$ of a discrete-time signal $x(n)$ as follows

$$X(z) = Z(x(n)) = \sum_{n=-\infty}^{\infty} x(n)z^{-n}$$

where n is an integer and z , a complex number.

Now if we take the z transform of the both sides of the equation, we obtain:

$$Y(z) = (1 + \alpha z^{-k})X(z)$$

Definition 2.3.1 *The transfer function of the FIR comb filter is*

$$H(z) = \frac{Y(z)}{X(z)} = 1 + \alpha z^{-k} = \frac{z^k + \alpha}{z^k}$$

Now the equation for the frequency response of discrete-time system is expressed by substituting $z = e^{j\omega}$. Therefore the frequency response for FIR comb filter

$$H\left(e^{j\omega}\right) = 1 + \alpha e^{-j\omega k}.$$

The zeros of the transfer function $H(z)$ are the solutions of the equation (assuming $0 < \alpha \leq 1$):

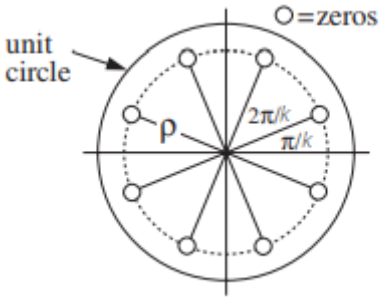

Figure 2.6: Pole−zero plot of FIR comb filter

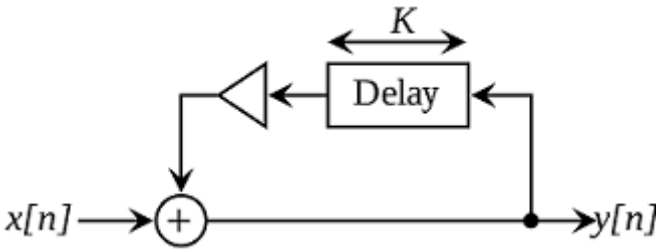

Figure 2.7: IIR comb filter structure [10].

$$1 + \alpha z^{-k} = 0 \Rightarrow z_m = \rho e^{\pi j(2m+1)/k},\ m = 0, 1, ..., k-1$$

where $\rho = \alpha^{1/k}$. The zero pattern are shown in Fig. (2.6).

The Infinite Impulse Response (IIR) comb filter adds a delayed version of the output signal of the filter to the input signal as shown in Fig. (2.7), and is represented by the equation:

$$y(n) = x(n) + \alpha y(n-k)$$

with $|\alpha| < 1$

If we rearrange this equation so that all terms in y are on the left-hand side, and then take the z transform, we obtain:

$$\left(1 - \alpha z^{-k}\right) Y(z) = X(z)$$

Definition 2.3.2 *The transfer function of the IIR comb filter is*

$$H(z) = \frac{Y(z)}{X(z)} = \frac{1}{1 - \alpha z^{-k}} = \frac{z^k}{z^k - \alpha}$$

and the frequency response is given by

$$H\left(e^{j\omega}\right) = \frac{1}{1 - \alpha e^{-j\omega k}}$$

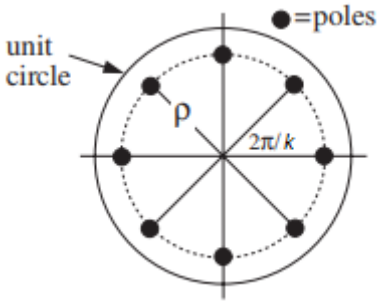

Figure 2.8: Pole−zero plot of IIR comb filter

The transfer function has poles at $p_m = \rho e^{j\omega m}$, $m = 0, 1, ..., k-1$, where $\omega_m = 2\pi m/k$ and $\rho = \alpha^{1/k}$. They are spaced equally around the circle of radius ρ, as shown in Fig. (2.8)

Remark 2.3.1 *When viewed from the z-plane is that ω represents L number of points on the unit circle (when $\alpha = 1$), equally subdivided into $2\pi/L$ angular increments. But we can see that for $|\alpha| < 1$, the poles in the z-plane will be inside the unit circle which guarantees stability for the IIR comb-filter.*

Notch Filters

A notch filter is a type of bandstop filter that reduces a narrow range of frequencies. And it is similar to a comb filter, but rather than having multiple evenly spaced stopbands, it has only a single stopband. Notch Filters are used in Raman spectroscopy, confocal or multi-photon microscopy, laser-based fluorescence instrumentation, or other life science applications.

The second-order "resonator" filter whose frequency response is dominated by a single narrow pole peak at some frequency ω_0, which is shown in Fig. (2.9)

Place a pole inside the unit circle along the ray to make a peak at $\omega = \omega_0$, hence

$$p = Re^{j\omega_0}$$

and the conjugate

$$p^* = Re^{-j\omega_0}$$

where the pole magnitude is $0 < R < 1$. And place a pair of zeros near the poles along the same directions as the poles, that is, at locations:

$$z_1 = re^{j\omega_0}, \quad z_1^* = re^{-j\omega_0}$$

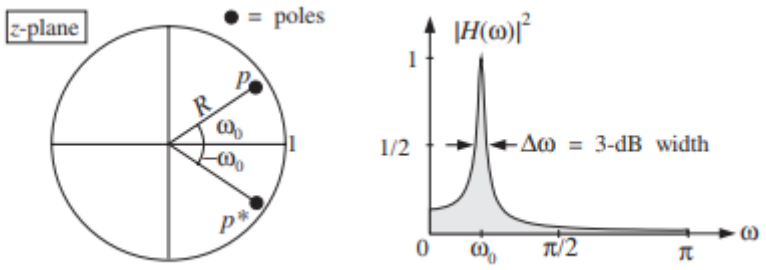

Figure 2.9: Pole/zero pattern and frequency response of the filter [19].

where r is restricted to the range $0 \leq r \leq 1$ so the transfer function can be written as

$$H(z) = \frac{(1 - re^{j\omega_0}z^{-1})(1 - re^{-j\omega_0}z^{-1})}{(1 - Re^{j\omega_0}z^{-1})(1 - Re^{-j\omega_0}z^{-1})} = \frac{1 + b_1z^{-1} + b_2z^{-2}}{1 + a_1z^{-1} + a_2z^{-2}}$$

where a_1 and a_2 are related to R and ω_0 by

$$a_1 = -2Rcos\omega_0, \quad a_2 = R^2$$

$$b_1 = -2rcos\omega_0, \quad b_2 = r^2$$

For a notch filter $r = 1$ the coefficients can be written as

$$a_1 = Rb_1 = -2Rcos\omega_0, \quad a_2 = R^2b_2 = R^2$$

And the transfer function takes the form

$$H(z) = \frac{1 + b_1z^{-1} + b_2z^{-2}}{1 + Rb_1z^{-1} + R_2b_2z^{-2}} = \frac{N(z)}{N(R^{-1}z)}$$

$$= \frac{\prod_{i=1}^{M} 1 - e^{j\omega_i}z^{-1}}{\prod_{i=1}^{M} 1 - e^{j\omega_i}\rho z^{-1}}$$

where $N(z)$ have zeros at the two notch locations $z = e^{\pm j\omega_0}$, and for some parameter $0 < \rho < 1$, The zeros of $N(R^{-1}z)$ lie at the same directions as the notch zeros, but they are all pushed inside the unit circle at radius ρ. Therefore, for each desired zero $z_i = e^{j\omega_i}$, there is a corresponding pole $p_i = \rho e^{j\omega_i}$.

And the transfer function becomes

$$H(z) = \frac{N(z)}{N(\rho^{-1}z)} = \frac{1 + b_1z^{-1} + b_2z^{-2} + \cdots + b_Mz^{-M}}{1 + \rho b_1z^{-1} + \rho^2b_2z^{-2} + \cdots + \rho^Mb_Mz^{-M}}$$

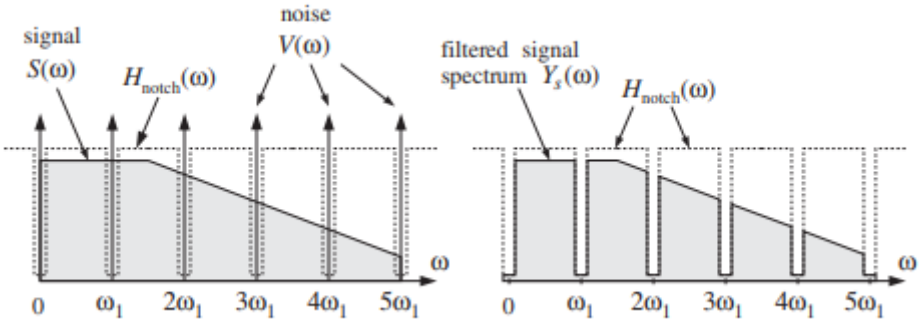

Figure 2.10: Notch filter for reducing periodic interference [19].

that is, the denominator coefficients are chosen as the scaled versions of the numerator coefficients,

$$a^i = \rho_i \quad b_i, i = 1, 2, \cdots, M$$

2.4 TV and Video Comb Filters

The lowest frequency of a periodic waveform called a fundamental frequency, most of a periodic wave have more than one frequency and those used in musical instruments typically vibrate at harmonics of the fundamental frequency, a harmonic is defined as an integer multiple of the fundamental frequency. In the equation $x(n) = s(n) + v(n)$, the noise signal $v(n)$ is periodic, and its spectrum is concentrated at the harmonics of a fundamental frequency.

Example 2.4.1 *Fig.(2.10) shwos an ideal notch filter to reduce the noise with notches at these harmonics. Moreover, the desired signal $s(n)$ is periodic and the noise is a wideband signal.*

Example 2.4.2 *Fig.(2.11) shows an ideal comb filter to enhance the signal with peaks at the harmonics of the desired signal.*

When one filter is one, and the other filter is zero, so that their frequency responses add up to unity. Hence, the ideal notch and comb filters are complementary filters

$$H_{notch}(\omega) + H_{comb}(\omega) = 1 \tag{2.9}$$

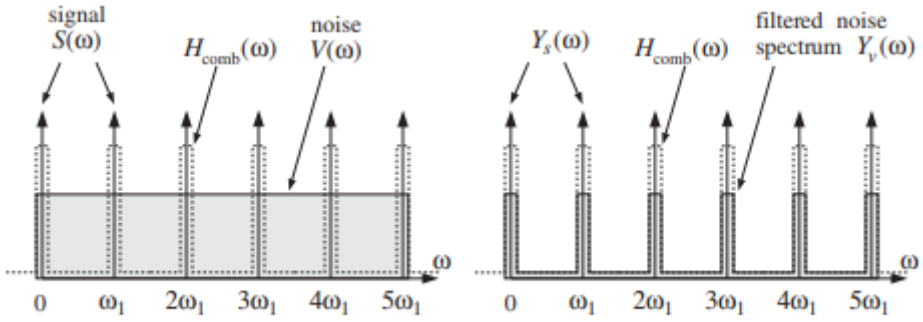

Figure 2.11: Comb filter for enhancing periodic signal [19].

A typical application of the notch case is the 60 Hz power−frequency interference picked up through insufficiently shielded instrumentation. This problem is especially acute in biomedical applications, such as measuring an electrocardiogram (ECG) by chest electrodes−a procedure which is prone to such interference. The literature on biomedical applications of DSP is extensive, with many filter design methods that are specialized for efficient microprocessor implementations.

A Comb Filter for Periodic Noise Reduction

A comb filter is used to eliminate a periodic noise signal from an observed signal to extract the desired signal. A major application of this idea is in color TV, digital video systems, and proposed HDTV systems .

Definition 2.4.1 *A composite video signal is made up of separate luminance and chroma signals, the luminance signal represents the black and white portion of the video picture, and the chroma signal represents the color portion of the picture.*

The chroma signal is comprised of separate I and Q components that result from mixing the separate colors, and responsible for adding color to the objects formed by the luminance signals [2].

Proposition 2.4.1 *The chroma I and Q components are combined within the same bandpass as the luminance, in order to be suitable with blake and white receivers and existing bandwidth requirements.*

Example 2.4.3 *Fig. (2.12) shwos the combined chroma I and Q components within the same bandpass as the luminance.*

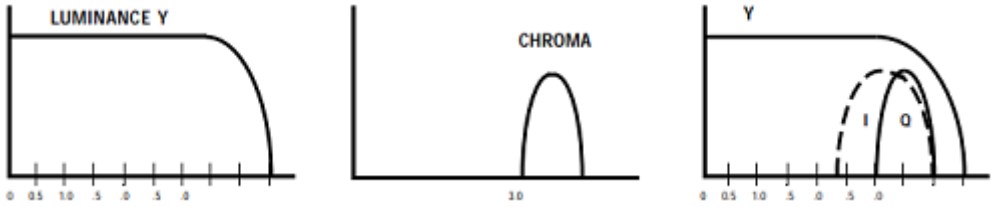

Figure 2.12: Luminance and Chroma signals

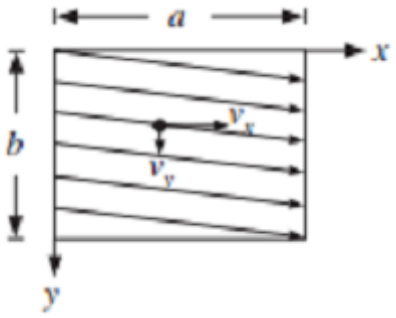

Figure 2.13: Scanned image

A very useful technique for faithful reproduction of original picture quality is the comb filtering process. The discrete nature of the frequency spectrum, due to vertical and temporal sampling, as well as the different locations of the luminance and chrominance components, make it feasible to adapt the response of special designed comb filter structures to separate them conveniently. Spectra separation in the receiver is based on the color subcarrier phase inversion from line to line and from frame to frame. This subcarrier characteristic is required for keeping compatibility between the color standard and Black and white standard.

Assume there are N horizontal scan lines in the two-dimensional still picture of horizontal and vertical dimensions a and b, as shown in Fig. (2.13). And if T_H is the time to scan one line, then the time to scan the complete picture (i.e., one frame) is equal to the scanning time for N lines, that is,

$$T_F = NT_H.$$

The quantities T_H and T_F are called the line and frame delays, and their inverses are the line and frame rates:

$$f_H = \frac{1}{T_H}, \quad f_F = \frac{1}{T_F}$$
$$\Rightarrow f_H = Nf_F \tag{2.10}$$

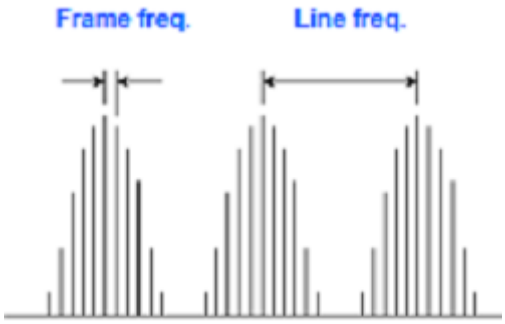

Figure 2.14: macro-structure and a micro-structure of a video spectrum

The frequencies f_H and f_F are associated to the horizontal and vertical velocities of the scanning point by

$$f_H = \frac{v_x}{a}, \quad f_F = \frac{v_y}{b} \tag{2.11}$$

Where f_H-harmonics represent the horizontal variations in the image, and the f_F-harmonics the vertical variations.

Example 2.4.4 *There are two levels of detail in Fig. (2.14), the peaks at integer multiples of the line rate f_H, the "macrostructure" represent the horizontal detail in the image. Between each pair of line rate peaks there is a "microstructure" frequencies spaced at the frame rate f_F, these represent the vertical detail of the image. In fact, if the microstructures all had zero amplitude, then the case of identical scan lines with no vertical detail.*

Let us first consider the usual expression of the image field as a single Fourier series, the picture will be considered as a "still" so that entire successive scannings are identical. The brightness or illumination of the field is a function $g(x, y)$ of both x and y, along any horizontal line (in the x direction, constantly keeping $y = y_1$) the illumination may be expressed as a single Fourier series

$$g(x, y_1) = \sum_k C_k e^{2\pi jkx/a}$$

Along any other line in the x direction a similar series holds with different coefficients, that is, the C's are functions of y. therefore each be written as a Fourier series along y

$$C_k = \sum_m C_{km} e^{2\pi jmy/b}$$

which gives the double Fourier series,

$$g(x,y) = \sum_{km} C_{km} e^{2\pi jkx/a} e^{2\pi jmy/b}$$

Where k and m correspond to the horizontal and vertical variations in $g(x,y)$ where

$$f_{km} = kf_H + mf_F \tag{2.12}$$

A scanned picture with a uniformly moving scanning spot is obtained by replacing $x = v_x t$, $y = v_y t$ and using Eq. (2.11) resulting in the video signal

$$\begin{aligned} V(t) &= g(v_x t, v_y t) \\ &= \sum_{km} C_{km} e^{2\pi jkv_x t/a} e^{2\pi jmv_y t/b} \\ &= \sum_{km} C_{km} e^{2\pi jkf_H t} e^{2\pi jmf_F t} \\ &= \sum_{km} C_{km} e^{2\pi jf_{km} t} \end{aligned}$$

Theorem 2.4.1 *The spectra of the chrominance signals will be shefted and centered about the subcarrier frequency f_{sc}, by the subcarrier modulation. If the frequencies of the modulated chrominance signal is at:*

$$f_{sc} + f_{km} = f_{sc} + kf_H + mf_F \tag{2.13}$$

then

$$f_{sc} = (d_F + \frac{1}{2}) f_F = \frac{1}{2}(2d_F + 1) f_F \tag{2.14}$$

Proof:
By choosing f_{sc} to be a half-multiple of the line frequency f_H, the chrominance peaks will fall exactly half-way between the luminance peaks, we can take for example,

$$f_{sc} = (d_H + \frac{1}{2}) f_H = \frac{1}{2}(2d_H + 1) f_H \tag{2.15}$$

Therefore, the chrominance macro-structure peaks are centered at half-multiples of f_H:

$$f_{sc} + f_{km} = (d_H + k + \frac{1}{2}) f_H + mf_F$$

since $f_H = Nf_F$ then

$$f_{sc} = (d_H + \frac{1}{2})f_H = (d_H + \frac{1}{2})Nf_F$$

and

$$f_{sc} = (d_F + \frac{1}{2})f_F = \frac{1}{2}(2d_F + 1)f_F$$

where

$$d_F + \frac{1}{2} = (d_H + \frac{1}{2})N$$

Moreover

$$f_{sc} + f_{km} = kf_H + (d_F + m + \frac{1}{2})f_F$$

Remark 2.4.1

1. *A few problems and challenges occur to video equipment since luminance and chroma signals sharing the same frequency spectrum, which must be separated. When a video signal have a high frequency luminance content, the luminance and chroma sidebands may overlap. And, when this high frequency luminance signals get into the chroma circuits, they simulate color information and are processed by the color circuits. which causes wrong colors in some parts of the picture or color swirls. This mostly happens when the spacing between the objects in the picture repeat at a frequency near 3.58 MHz.*

2. *But when using the comb filter the main operation be divided into two parts. At first, the comb filter remove the luminance information from the composite video signal leaving only the chroma signal and its sidebands. Second, the "combed" chroma is used to remove the color from the original composite video, leaving only the luminance information. By these process we get a clean luminance and chroma signals, which require for a high resolution picture.*

3. *In the digital processing of television signals the choice of the sampling rate is more significant than in the digital processing of other types of signal. This is closely related to the special features of TV signals such as the breakdown of a scene into lines and fields and the way in which the colour information is coded.*

Theorem 2.4.2 *Let the chrominance and luminance separation be resampled to four times the subcarrier frequency, that is, If*

$$f_s = 4f_{sc}$$

then

$$f_s = 2(2d_H + 1)f_H = D_H f_H \tag{2.16}$$

where

$$D_H = 2(2d_H + 1)$$

and

$$f_s = 2(2d_H + 1)f_H = D_H f_H \tag{2.17}$$

where

$$D_F = 2(2d_F + 1)$$

Proof
using Eqs. (2.15) and (2.14), the sampling rate will given as

$$f_s = 4f_{sc} = 2(2d_H + 1)f_H = D_H f_H$$

where

$$D_H = 2(2d_H + 1)$$

and

$$f_s = 4f_{sc} = 2(2d_F + 1)f_F = D_F f_F$$

where

$$D_F = 2(2d_F + 1)$$

$$D_F = ND_H$$

4. *In units of radians per sample, the subcarrier frequencyf_{sc} becomes*

$$\omega_{sc} = \frac{2\pi f_{sc}}{f_s} = \frac{2\pi f_{sc}}{4f_{cs}} = \frac{\pi}{2}$$

Similarly,

$$\omega_F = \frac{2\pi f_F}{f_s} = \frac{2\pi f_F}{D_F f_F} = \frac{2\pi}{D_H}$$

and

$$\omega_H = \frac{2\pi f_H}{f_s} = \frac{2\pi f_H}{D_F f_H} = \frac{2\pi}{D_H}$$

by using Eqs. (2.17) and (2.18), the luminance video frequencies f_{km} become

$$\omega_{km} = \frac{2\pi f_{km}}{f_s} = \frac{2\pi k f_H}{D_H f_H} + \frac{2\pi m f_F}{D_F f_F} = \frac{2\pi k}{D_H} + \frac{2\pi m}{D_F} = K\omega_H + m\omega_F$$

5. *The shifted chrominance frequencies can be expressed as half-multiples either the line or the frame digital frequencies*

$$\omega_{sc} + \omega_{km} = (2d_H + 2k + 1)\frac{\pi}{D_H} + \frac{2\pi m}{D_F}$$

$$= \frac{2\pi k}{D_H} + (2d_F + 2m + 1)\frac{\pi}{D_F}$$

$$= (2kN + 2d_F + 2m + 1)\frac{\pi}{D_F}$$

6. *The comb filters used in video systems is the basic comb filter*

$$H(z) = \frac{b}{1 - az^{-1}},$$

where b is the overall gain. The signal band will only be the DC frequency $\omega = 0$. therefore, we require, that the filter have unity response at $\omega = 0$ or equivalently at $z = 1$.

The NRR of the filter can be improved slightly, without affecting the speed of response, by adding a zero in the transfer function at $z = -1$. The resulting filter will be:

$$H(z) = b\frac{(1 + z^{-1})}{1 - az^{-1}}$$

$$H(1) = \frac{2b}{1 - a} = 1$$

$$b = \frac{1 - a}{2}$$

7. *To obtain a multi-comb filter substitut*

$$z \to z^D$$

that is,

$$H(z) = b\frac{1 - z^{-1}}{1 - az^{-1}} \quad \Rightarrow \quad H(z^D) = b\frac{1 - z^{-D}}{1 - az^{-D}}$$

where D can be either a line delay $D = D_H$ or a frame delay $D = D_F$

The effect of this substitution is the D-fold replication of the spectrum of the original filter

$$H(\omega) \longrightarrow H(D\omega)$$

8. *This transformation shrinks the original spectrum $H(\omega)$ by a factor of D and replicates it D times. Because the spectrum $H(\omega)$ has period $0 \leq \omega \leq 2\pi$, the new spectrum $H(D\omega)$ will have period $0 \leq \omega D \leq 2\pi$, which becomes the scaled period $0 \leq \omega \leq 2\pi/D$ fitting exactly D times into the new nyquist interval $0 \leq \omega \leq 2\pi$.*

   The filter parameters are chosen to have simple values, because of the high sampling rates involved, to minimize the computational cost. For example, the simplest choice is the following FIR comb filter, obtained by setting $a = 0$ and $b = 1/2$

$$H_{comb}(z) = \frac{1}{2}(1 + z^{-D})$$

   using the complementary property of notch and comb filters Eq. (2.9)

$$H_{notch}(z) = \frac{1}{2}(1 - z^{-D})$$

Note: If D is a line delay, $D = D_H$, then the peaks of $H_{comb}(z)$ will coincide with the macrostructure line-frequency peaks of the luminance signal , and its notches will coincide with the macro-structure peaks of the modulated chrominance signal . Thus, filtering the composite video signal through $H_{comb}(z)$ will tend to remove the chrominance sigal and let the luminance signal pass through, at least at the macro-structure level which is the dominant part the spectrum. Conversely, if D is a frame delay, $D = D_F$, then the filtering of the composite video signal through $H_{notch}(z)$ will tend to remove the luminance sigal and let the chrominance signal pass through. Thus, the two filters can be used in parallel to extract the chrominance and liminance components.

Comb filters fail in two ways. At first, some outputs may get lost, a good black and white picture will produce if the chroma output is missing. Second, bad component or a change in the comb filter′s alignment causes the signals to separate incorrectly which produce a worse picture than the ordinary filter.

Example 2.4.5 *we apply the IIR filter (butter filter from mathlab,see appendix) to extract a signal of the form*

$$x(n) = v(n) + s(n)$$

where v(n) is zero-mean white Gaussian noise of variance σ_v^2 . And s(n) is the sum of sinusoidal signals

$$s(n) = 5sin(2\pi f_1 n)$$

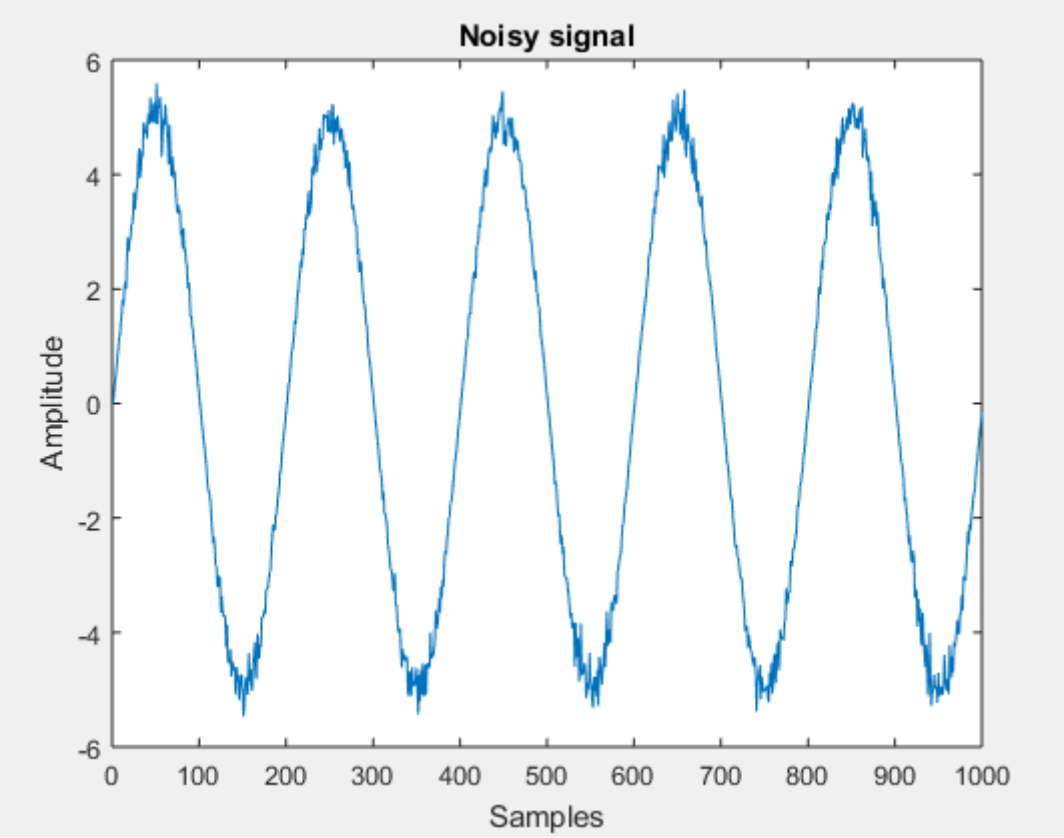

Figure 2.15: Noisy input signal

where $f_1 = 1KHz$. *We apply this filter with normalized cutoff frequencies* $a = 0.1$, $a = 0.4$ *and* $a = 0.8$. *the result are shown in Figs. (2.15), (2.16), (2.17) and (2.18)*

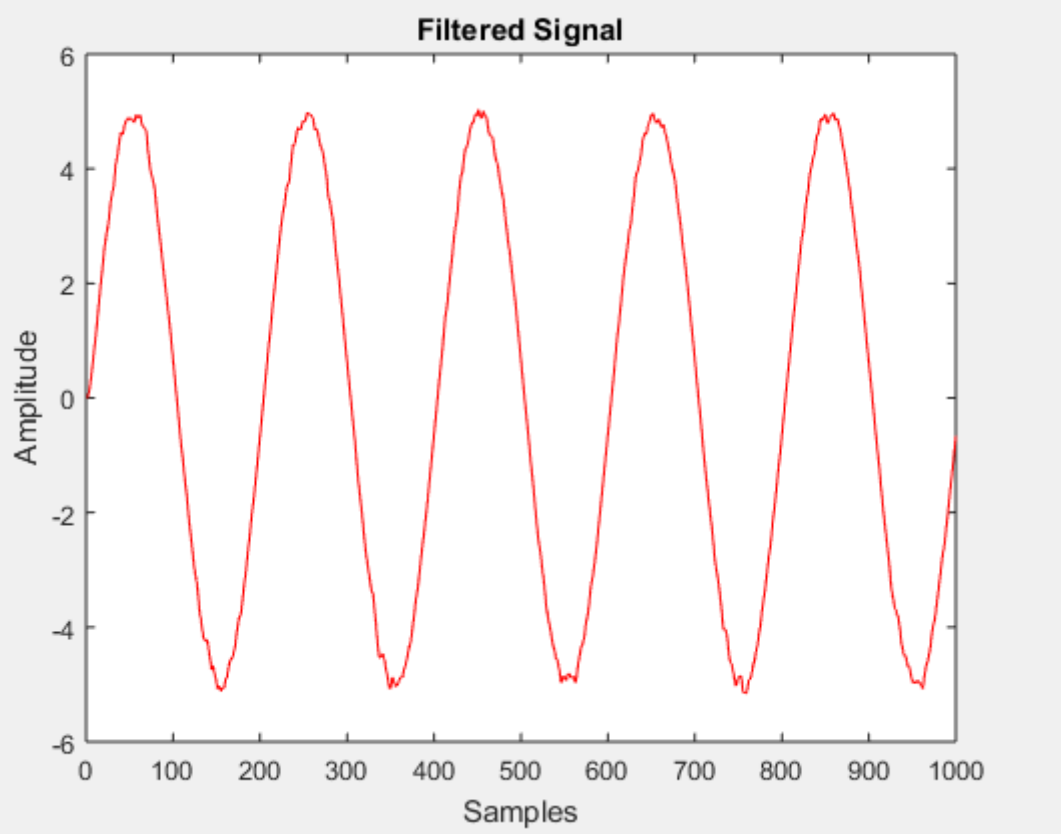

Figure 2.16: Filtered signal,for a=0.1

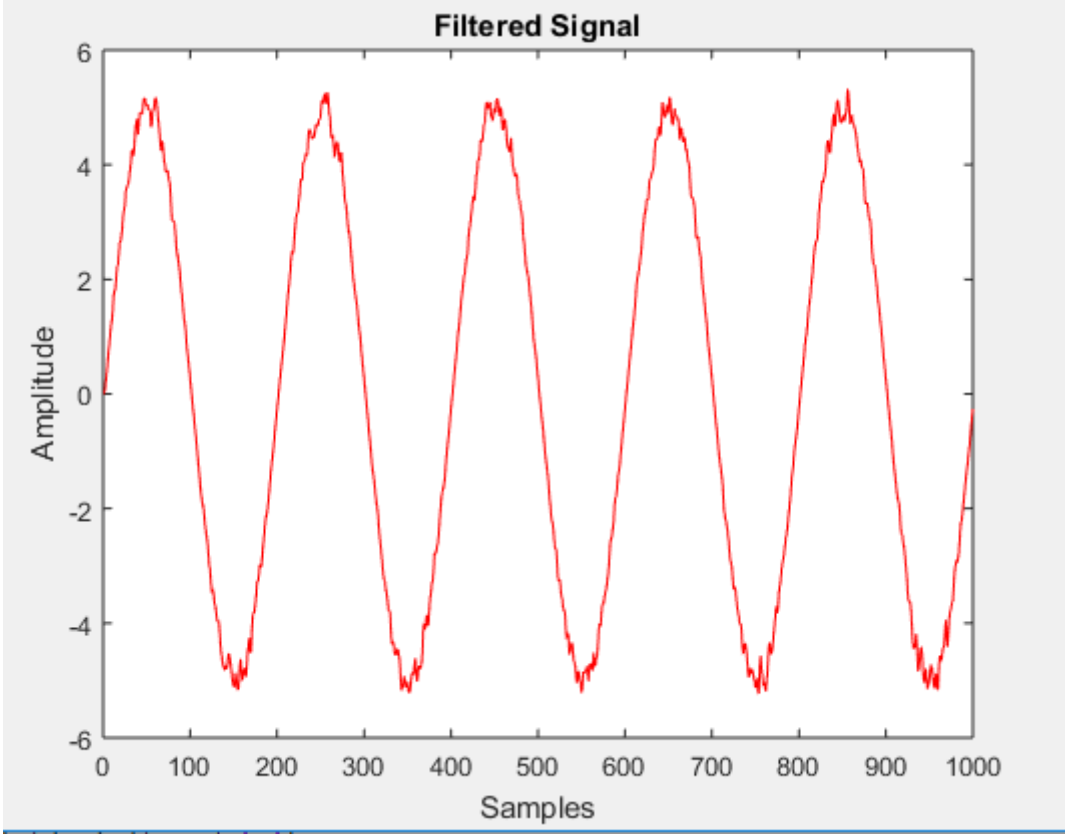

Figure 2.17: Filtered signal,for a=0.4

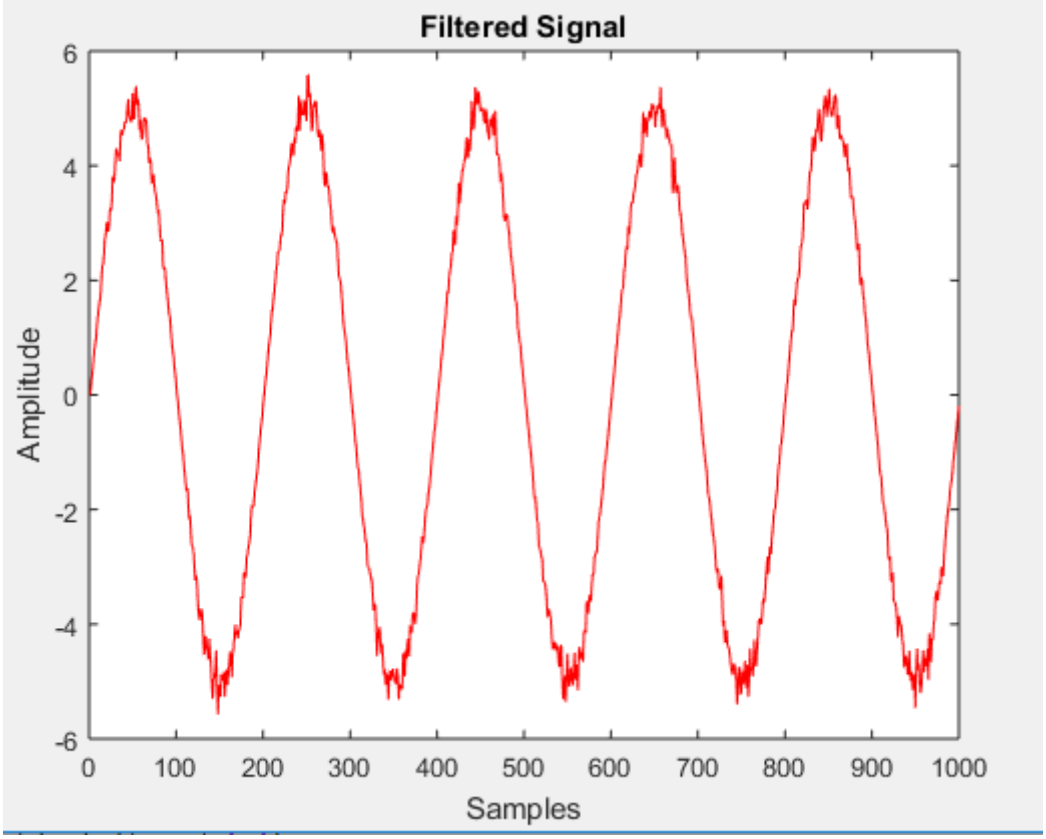

Figure 2.18: Filtered signal,for a=0.8

Chapter 3

Geometrical and Variational PDEs in Image Processing

The applications of partial differential equations (PDEs) to computer vision and image processing date back to the 1960s [9]. But, this method using (PDEs) did not get much attention until the introduction of the notion of scale space by Koenderink and Witkin in the 1980s. Perona and Maliks work on non linear diffusion also open the way for great attention towards PDE-based method. Nowadays, PDEs have been successfully applied to many problems in image processing and computer vision [5].

There are many approaches have been studied to develope image processing, and it is hard to say which one is butter than the other. The oldest methods to study the image processing could be 1-D signal processing techniques. PDEs, which belong to one of the most important parts of mathematical analysis, are closely related to the physical world. Every scientist comes across the wave equation or the heat equation, and the names of Euler, Poisson, Laplace, etc., are quite familiar.

One of the basic important tasks of image processing is denoising, which means the process with which we reconstruct a signal from a noisy one, by removing unwanted noise, in order to restore the original image. For theoretical purposes it is often assumed that an image L is the result of the superposition of a real informational content L and noise n. The main aim of a denoising algorithm is to reduce the noise level, while preserving the image features. So image denoising is still a challenging task for the investigators. Several methods are being developed to perform denoising of corrupted images [26].

This chapter focuses on the theme of image denoising and enhancement of several PDE-based image denoising and enhancement model for analysis and improvement. It discusses simplifing PDE using gauge coordinates - second-order deriva-

tives in local coordinates. It depends on the norm of the gradient and a linear combination of the two second order derivatives in gauge directions. Moreover it discusses the anisotropic diffusion method and diffusion equation with a nonlinear structure. It also investigates general geometric PDEs depending on second order derivatives in the qualitative behaviour of the PDE. Furthermore, it considers special structures such as undefined points which occurs at critical points and ridges. And it present a numerical schemes for both noise-constrained and unconstrained evolution.

3.1 Using PDEs in Image Processing

In the variational or "energy" based models, nonlinear PDEs emerge as one derives formal Euler Lagrange equations or tries to locate local or global minima by the gradient descent method. Some PDEs can be studied by the viscosity solution approach , while many others still remain open to further theoretical investigation. Compared with other approaches, the variational PDE method has remarkable advantages in both theory and computation. It allows one to directly handle and process visually important geometric features such as gradients, tangents, curvatures, and level sets. It can also effectively simulate several visually meaningful dynamic processes, such as linear and nonlinear diffusions and the information transport mechanism.

Gauge coordinates

An image can be thought of as a collection of curves with equal value, the isophotes. Most isophotes are non-self-intersecting. At extrema an isophote reduces to a point, at saddle points the isophote is self-intersecting. At the non-critical points gauge coordinates (v, w) can be chosen. Gauge coordinates are locally set such that v points in the tangential direction of the isophote, and w in the orthogonal direction [12], i.e., in the direction of the image gradient (the directional change in the intensity or color in an image) as shown in Fig. (3.1). So in every pixel we have a differently oriented v, w frame attached to the image. The important notion is that any derivative with respect to v and w is invariant under translation and rotation, and so any combination of such gauge derivatives. So, $\frac{\partial L}{\partial w}$ (where L is the image intensity function) is the gradient magnitude. And $\frac{\partial L}{\partial v} = 0$, as there is no change in the luminance as we move tangentially along the isophote.

$$w = \begin{pmatrix} L_x \\ L_y \end{pmatrix}$$

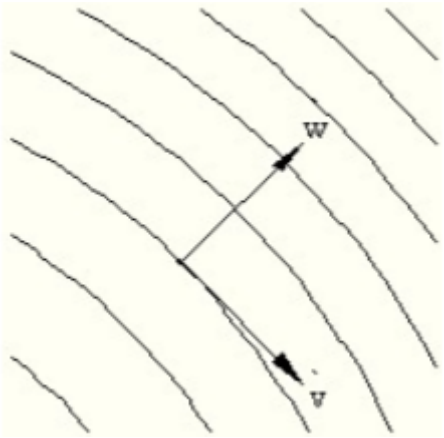

Figure 3.1: The unit vectors in the gradient and tangential direction are w and v

$$v = \begin{pmatrix} cos\frac{\pi}{2} & sin\frac{\pi}{2} \\ -sin\frac{\pi}{2} & cos\frac{\pi}{2} \end{pmatrix} \cdot w$$
$$= \begin{pmatrix} 0 & 1 \\ -1 & 0 \end{pmatrix} \cdot \begin{pmatrix} L_x \\ L_y \end{pmatrix} = \begin{pmatrix} L_y \\ -L_x \end{pmatrix}$$

as v is perpendicular to w.

As we denote the derivative of an image in the x direction by L_x, we adopt a similar notation for derivatives in the v or w direction. For example, the first derivative of L in the w direction is denoted by L_w, the second by L_{ww}, *etc.* The derivative of L in the direction of a certain row vector is defined as

$$L_a = \frac{1}{\|a\|}(a \cdot \bigtriangledown)L$$

where $\bigtriangledown$ is the Nabla vector defined by $\bigtriangledown = \begin{pmatrix} \frac{\partial}{\partial x} \\ \frac{\partial}{\partial y} \end{pmatrix}$, and the dot $(\cdot)$ denotes the inner product. Then

$$\begin{aligned} L_w &= \frac{1}{\sqrt{L_x^2 + L_y^2}} \left((L_x \quad L_y) \cdot \begin{pmatrix} \frac{\partial}{\partial x} \\ \frac{\partial}{\partial y} \end{pmatrix} \right) L \\ &= \frac{L_x L_x + L_y L_y}{\sqrt{L_x^2 + L_y^2}} \\ &= \sqrt{L_x^2 + L_y^2}\,, \end{aligned}$$

and

$$\begin{aligned} L_v &= \frac{1}{\sqrt{L_x^2 + L_y^2}} \left((L_y \quad -L_x) \cdot \begin{pmatrix} \frac{\partial}{\partial x} \\ \frac{\partial}{\partial y} \end{pmatrix} \right) L \\ &= \frac{L_y L_x - L_x L_y}{\sqrt{L_x^2 + L_y^2}} \\ &= 0. \end{aligned}$$

Theorem 3.1.1 *The second order directional derivatives can be computed as follows:*

$$L_{aa} = \frac{1}{\|a\|^2}(a \cdot \bigtriangledown)^2 L.$$

Proof:

$$\text{let } M = L_a, \text{ then } L_{aa} = M_a,$$

Now

$$M = \frac{1}{\|a\|}(a \cdot \bigtriangledown)L.$$

Hence

$$\begin{aligned} M_a &= \frac{1}{\|a\|}(a \cdot \bigtriangledown)M \\ &= \frac{1}{\|a\|}(a \cdot \bigtriangledown)\frac{1}{\|a\|}(a \cdot \bigtriangledown)L \\ &= \frac{1}{\|a\|^2}(a \cdot \bigtriangledown)^2 L. \end{aligned}$$

Therefore

$$l_{aa} = \frac{1}{\|a\|^2}(a \cdot \bigtriangledown)^2 L.$$

Corollary 3.1.1 *Substituting $a = v$ and $a = w$ we get respectively the second derivatives*

$$L_{vv} = \frac{L_x^2 L_{yy} + L_y^2 L_{xx} - 2L_x L_y L_{xy}}{L_x^2 + L_y^2}. \tag{3.1}$$

$$L_{ww} = \frac{L_x^2 L_{xx} + L_y^2 L_{yy} + 2L_x L_y L_{xy}}{L_x^2 + L_y^2}. \tag{3.2}$$

Note: These gauge derivatives can be expressed as a product of gradients and a 2×2 matrix with second-order derivatives:

$$L_{ww}L_w^2 = (L_x\ ,\ L_y)\begin{pmatrix} L_{xx} & L_{xy} \\ L_{xy} & L_{yy} \end{pmatrix}\begin{pmatrix} L_x \\ L_y \end{pmatrix},$$

$$L_{vv}L_w^2 = (L_x\ ,\ L_y)\begin{pmatrix} L_{yy} & -L_{xy} \\ -L_{xy} & L_{xx} \end{pmatrix}\begin{pmatrix} L_x \\ L_y \end{pmatrix}.$$

For L_{ww} the matrix equals the Hessian H. For L_{vv} it is $(detH)\cdot(H^{-1})$ Furthermore, one gets the Laplacian

$$\triangle L = \bigtriangledown^2 L = \frac{\partial^2 L}{\partial v^2} + \frac{\partial^2 L}{\partial w^2} = L_{vv} + L_{ww}.$$

Gaussian scale space

The key to detecting an operator to a particular scale seems to be changing the image resolution. Which can be decreased by merging the grey values of a block of pixels into the new grey value of a larger pixel. This technique of lowering the resolution to bring large-scale structures into kernel range and remove small-scale structures, is a much-used and easy to perform by using the convolution with a Gaussian. Which lowers the resolution but does not insert new details into the image, Fig. (3.2).

Scale space started in 1983 by a paper of Witkin [32], discussing the blurring properties of one dimensional signals. After that, Koenderink intoduce a method to study the dependence of image structure on the level of resolution, he focussed on the linear heat equation.

Let $L(x) : \mathbb{R}^n \longrightarrow \mathbb{R}$ be an image with x an n-dimensional spatial variable (point) and $L(x)$ the intensity measured at a point x. The Gaussian scale-space image $L(x,t)$ is defined as the convolution of L with a Gaussian [14]:

$$L(x,t) = \int_{\mathbb{R}^n} \frac{1}{(\sqrt{4\pi t})^n} e^{-\frac{|x-y|^2}{4t}} L(y)dy$$

The causality is a notion implies the non-enhancement of local extrema: everything is flattened. So the intensity of minima increases and that of maxima decrease. Meanwhile, all eigenvalues are negative and positive, respectively. The sum of the eigenvalues equals the trace of the Hessian. For simplicity taking a 2D image L(x, y), the trace of the Hessian is $L_{xx} + L_{yy}$, which is $\triangle L$. Then the causality principle states that at maxima $\triangle L < 0$ (being the sum of the eigenvalues) and

Figure 3.2: Lowering the resolution by Gaussian convolution, [17].

$L_t < 0$ (decreasing intensity for increasing scale). At minima the opposite holds: $\triangle L > 0$ and $L_t > 0$. And thus, in all cases, $\triangle L \cdot L_t > 0$. Clearly, this work for any dimension. Hence, n- dimensional image can be extended to an$(n+1)$-dimensional image $L(x,t)$, with $x \in \mathbb{R}^n$. Imposing the linearity between $\triangle L$ and L_t yields $\triangle L = \alpha L_t$, with $\alpha > 0$, without loss of generality the simplest solution that we may take is when $\alpha = 1$. This results in the differential equation

$$\begin{cases} L_t(x,t) = \triangle L(x,t) \\ \lim_{t \downarrow 0} L(x,t) = L_0(x) \end{cases}$$

Example 3.1.1 *Fig. (3.2) shows lowering the resolution by Gaussian convolution, taking all images at all widths (scales) yields a Gaussian scale-space image. Note that by lowering the resolution some details vanish from the images. Hence, image processing is not satisfactory by applying a Gaussian scale space. In particular, if one wants to detects edges in images. Hence, many non-linear diffusion equations were introduced. Some of them will be given in the next sections.*

P-Laplacians

Consider in general the integral $E(L) = \int_\Omega \frac{1}{p} |\bigtriangledown L|^p d\Omega$, which is known as the p-Dirichlet energy integral with a companying p$-$Laplacian equation. The minimum is given by setting the variational derivative to zero: $\delta E(L) = 0$, with

$$\delta E = - \bigtriangledown \cdot (|\bigtriangledown L|^{p-2} \bigtriangledown L).$$

Using gauge coordinate, the integral can be written as

$$E(L) = \frac{1}{p} \int_\Omega L_w^p d\Omega$$

Theorem 3.1.2 *The variational derivative $\delta E(L)$ can be written as [14]*

$$\delta E(L) = -L_w^{p-2}((p-1)L_{ww} + L_{vv}).$$

Proof:
Let η be an arbitrary admissible function that vanishes on $\partial\Omega$. Then, by definition

$$\begin{aligned}\delta E(L,\eta) &= \frac{1}{p}\int_\Omega \frac{d}{d\epsilon}|\bigtriangledown(L+\epsilon\eta)|^p dx|_{\epsilon=0} \\ &= \int_\Omega |\bigtriangledown L|^{p-2}\bigtriangledown L\cdot\bigtriangledown\eta dx \\ &= \int_{\partial\Omega}|\bigtriangledown L|^{p-2}\bigtriangledown L\cdot\eta ds - \int_\Omega \bigtriangledown\cdot(|\bigtriangledown L|^{p-2}\bigtriangledown L)\eta dx\end{aligned}$$

since $\eta = 0$ on the boundary, the first integral vanishes and the Euler Lagrange equation $\delta E(L) = 0$ reads

$$-(\bigtriangledown\cdot(|\bigtriangledown L|^{p-2}\bigtriangledown L)) = 0$$

The left hand side equals the well known variational derivative of the Laplacian. An explicit expressions is obtained by applying the divergence operator to both terms, where gauge coordinates are used

$$\begin{aligned}-\bigtriangledown\cdot(|\bigtriangledown L|^{p-2}\bigtriangledown L) &= -\bigtriangledown(|\bigtriangledown L|^{p-2})\cdot\bigtriangledown L - |\bigtriangledown L|^{p-2}(\bigtriangledown\cdot\bigtriangledown L) \\ &= -(\bigtriangledown L_w^{p-2})\cdot\bigtriangledown L - L_w^{p-2}\bigtriangleup L\end{aligned}$$

For the first part we have

$$\begin{aligned}(\bigtriangledown L_w^{p-2})\cdot\bigtriangledown L &= (p-2)L_w^{p-3}\bigtriangledown L_w\cdot\bigtriangledown L \\ &= (p-2)L_w^{p-3}((\bigtriangledown L)HL_w^{-1})\cdot\bigtriangledown L\end{aligned}$$

where H is the Hessian matrix, and $((\bigtriangledown L)H)\cdot\bigtriangledown L = L_w^2 L_{ww}$. Therefore

$$(p-2)L_w^{p-3}L_w^{-1}L_w^2 L_{ww} = (p-2)L_w^{p-2}L_{ww}$$

and consequently we have

$$\delta E(L) = -((p-2)L_w^{p-2}L_{ww} + L_w^{p-2}\bigtriangleup L)$$

Using the identity $\bigtriangleup L = L_{vv} + L_{ww}$ this gives

$$\delta E(L) = -L_w^{p-2}((p-1)L_{ww} + L_{vv})$$

Definition 3.1.1 *The p-Laplacian PDE is obtained as a steepest decent evolution towards the solution* $L_t = -\delta E(L)$.

Example 3.1.2 *For $p = 2$ we have the Gaussian scale space [11], in this case,*

$$L_t = L_w^{2-2}((2-1)L_{ww} + L_{vv}) = L_{ww} + L_{vv} = \triangle L$$

Next, $p = 1$ gives the Total variation flow [24], for which

$$L_t = L_w^{1-2}((1-1)L_{ww} + L_{vv}) = L_w^{-1}L_{vv}$$

The case $p \to \infty$ is known as the infinite Laplacian, denoted by $\triangle_\infty L$ [3]. This type of flow can be applied to image inpainting [6].

Non- Linear Diffusion

There are a number of phenomena in the physical sciences that we associate with the idea of diffusion. The linear diffusion equation is the basic mathematical model that has been thoroughly studied in the last two centuries. Nonlinear diffusion equations have played an important role not only in theory but also in physics and engineering.

The diffusion equation is a partial differential equation. It is usually presented in a general form [31]

$$\partial_t L(x,t) = \bigtriangledown \cdot (C(L,x,t) \bigtriangledown L(x,t)) \tag{3.3}$$

where $L(x,t)$ is the density of the diffusing material at coordinate x and time t. $C(L,x,t)$ denotes the collective diffusion coefficient for density L . If the diffusion coefficient doesn′t depend on the density, i.e., C is constant, then Eq. (3.3) reduces to the following linear equation

$$L_t = C \triangle L \text{ for } x \in R^n, t > 0$$
$$L(x,0) = L_0(x) \text{ for } x \in R^n$$

which is called the heat equation and also describes the distribution of a heat in a given region over time. The heat equation is the canonical smoothing process, diffusing data at a constant rate in all directions. When applied to an image $L(x,0)$ of two space dimensions, the result is a blurred version $L(x,t)$ for $t > 0$. Noise may be eliminated, but at the cost of making edges fuzzy.

To modify the heat equation, replace the constant diffusion coeffcient of Eq. (3.3)

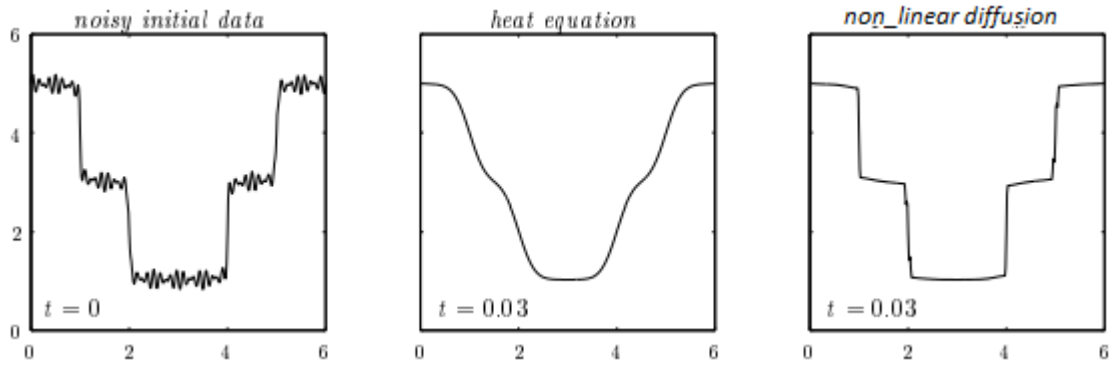

Figure 3.3: Edge enhancement,

by a nonlinear function of L that decreases to 0 as the gradient of L gets steeper. The non - linear diffusion is:

$$\begin{cases} L_t = \bigtriangledown \cdot (g(|\bigtriangledown L|) \bigtriangledown L) \ in \ \Omega \times (0, +\infty) \\ \dfrac{\partial L}{\partial n} = 0 \ in \ \partial\Omega \times (0, \infty) \\ L(x, 0) = L_0(x) \ in \ \Omega \end{cases} \tag{3.4}$$

Here Ω denotes picture domain. In general Ω is a bounded subset of $\mathbb{R}^n$. The function $g(.)$ is chosen such that, it enhances the edges (if $|\bigtriangledown L|$ is large, then the diffusion will be low and therefore the exact localization of the edge will be kept. if $|\bigtriangledown L|$ is small then the diffusion will tend to smooth still more around (x, y)), as shwon in Fig. (3.3).

A classical example is the Perona-Malik equation [20] where they replaced the constant diffusion coefficient of linear equation by a smooth nonincreasing diffusivity function g with $g(0) = 1,\ g(.) \geq 0$, and $\lim_{s\to\infty} g(.) = 0$. They conider the cases

$$g(|\bigtriangledown L|^2) = \frac{1}{1 + |\bigtriangledown L|^2/\lambda^2}$$

and

$$g(|\bigtriangledown L|^2) = exp\left(-\frac{|\bigtriangledown L|^2}{2\lambda^2}\right)$$

where λ corresponds to a contrast parameter (difference in the image intensities on the left and right) of the edge.

In the one-dimensional case, Perona-Malik introduce the flux function $\Phi(s) :=$

$sg(s^2)$, where $s = \bigtriangledown L(x,t)$ and $g(|s|^2) = \dfrac{1}{1+s^2/\lambda^2}$. As means to constrain the diffusion process to contiguous homogeneous regions, but not cross region boundaries.

Perona-Malik equation can be rewritten based on the flux function as follwos [20]:

$$L_t = \bigtriangledown \cdot \Phi(s) = \Phi'(L_x)L_{xx}$$

with

$$\Phi(s) = \frac{s}{1+s^2/\lambda^2}$$

Hence, $\Phi'(L_x)$ plays an important role in diffusion coefficient of the diffusion equation. To find $\Phi'(L_x)$

$$\Phi'(L_x) = \frac{\partial}{\partial_s}\left(\frac{s}{1+s^2/\lambda^2}\right) = \frac{1-s^2/\lambda^2}{(1+s^2/\lambda^2)^2}$$

Note: If $1-s^2/\lambda^2 < 0$, diffusion coefficient will be negative and it leads to backward diffusion that enhances contrasts of image intensity rather than smoothes them in image processing. Thus the Perona Malik model may sharpen edges if their gradient is larger than the contrast parameter λ.

Proposition 3.1.1 *In the two-dimensional case [29], Perona-Malik flux equation can be rewritten as*

$$L_t \;=\; g(|\bigtriangledown L|^2)(L_{vv}+L_{ww}) + 2g'(|\bigtriangledown L|^2)|\bigtriangledown L|^2 L_{ww}.$$

Proof:

$$\begin{aligned}
L_t &= \bigtriangledown \cdot (g(|\bigtriangledown L|^2)\bigtriangledown L) \\
&= g(|\bigtriangledown L|^2)\triangle L + 2g'(|\bigtriangledown L|^2)(L_xL_{xx}+L_yL_{yx},\ L_xL_{xy}+L_yL_{yy})\cdot\bigtriangledown L \\
&= g(|\bigtriangledown L|^2)\triangle L + 2g'(|\bigtriangledown L|^2)|\bigtriangledown L|^2 L_{ww} \\
&= g(|\bigtriangledown L|^2)(L_{vv}+L_{ww}) + 2g'(|\bigtriangledown L|^2)|\bigtriangledown L|^2 L_{ww}.
\end{aligned}$$

Since $\Phi'(s) = 2s^2\cdot g'(s^2) + g(s^2)$, now we have

$$L_t = \Phi'(|\bigtriangledown L|)L_{ww} + g(|\bigtriangledown L|^2)L_{vv}$$

Remark 3.1.1

1. *By taking $g(.) = 1$, the Gaussian scale space is obtained:*

$$L_t = \bigtriangledown \cdot ((1) \bigtriangledown L) = \bigtriangledown \cdot \bigtriangledown L = \triangle L.$$

2. *A general class of diffusion is obtained by [13], taking*

$$g(| \bigtriangledown L|) = \frac{1}{| \bigtriangledown L|^q}$$

then the diffusion becomes

$$L_t = \bigtriangledown \cdot (| \bigtriangledown L|^{-q} \bigtriangledown L).$$

3. *By taking $q = -p + 2$ the p-Laplacian is obtained*

$$L_t = \bigtriangledown \cdot (| \bigtriangledown L|^{p-2} \bigtriangledown L).$$

4. *For $q = 1$ one obtains the Total Variation flow [12]*

$$L_t = \bigtriangledown \cdot \left(\frac{\bigtriangledown L}{| \bigtriangledown L|} \right).$$

3.2 Geometry Driven Scale-Space Filtering

Let f be a scalar image defined on the spatial image domain Ω , then the family of diffused versions of f is given by [1]

$$U(f) : f(.) \longrightarrow L(\cdot, t) \quad with\ L(\cdot, 0) = f(\cdot)$$

where U is referred to as the scale-space filter, L is denoted by the scale-space image. The denoised or enhanced version of f is a given by $L(\cdot.t)$ that is the closest to the unknown noise-free version of f.

Mean Curvature Motion

In the last few decades, there has been increasing interest in mean curvature flows with applications in image processing (denoising, enhancement, segmentation). They showed that causal, local scale spaces are governed by PDEs and that under sound stability conditions for the scale space, the PDE′s have unique viscosity solutions. In particular all causal, local, isometric and contrast invariant scale spaces are given by curvature evolution equations [7]:

Definition 3.2.1 *curvature evolution equations ia an Euclidean shortening flow, which is given by*

$$\begin{aligned} L_t &= \bigtriangledown \cdot \left(\frac{\bigtriangledown L}{|\bigtriangledown L|} \right) |\bigtriangledown L| \\ &= \frac{L_x^2 L_{yy} + L_y^2 L_{xx} - 2L_x L_y L_{xy}}{L_x^2 + L_y^2}. \end{aligned}$$

As one can directly verify that Eq. (3.1) can be written as $L_t = L_{vv}$.

Edge Affected Variable Conductance Diffusion

Variable Conductance Diffusion (VCD) is a powerful method of image feature extraction in which blurring is allowed to occur except at edges, depending on a variable conduction coefficient that controls the rate of diffusion. However, the conductance coefficient edge affected-VCD is inversely proportional to the edgeness, which is known as the edge-stopping function, in which the edgeness is typically measured by the gradient magnitude. The Edge Affected Variable Conductance Diffusion is as follows:

$$L_t = \bigtriangledown \cdot (g(| \bigtriangledown L|) \bigtriangledown L)$$

Note that the Perona and Malik′s antitropic diffusion Eq.(3.4) is an Edge Affected Variable Conductance Diffusion.

Self-Snakes

Self - Snakes was proposed by Sapiro [25], which can be understood as nonlinear extension of mean curvature motion. The purpose was to prevent further shrinking of the level-lines once they have got to the significant image edges, to allow sharper edges.

$$L_t = | \bigtriangledown L| \bigtriangledown \cdot \left(g(| \bigtriangledown L|) \frac{\bigtriangledown L}{| \bigtriangledown L|} \right)$$

Which can be decomposed into two parts

$$L_t = g| \bigtriangledown L| \bigtriangledown \cdot \left(\frac{\bigtriangledown L}{| \bigtriangledown L|} \right) + (\bigtriangledown g) \cdot \bigtriangledown L$$

The first part describes a degenerate forward diffusion along the level lines that is orthogonal to the local gradient; it allows preserving the edges. Additionally,

the diffusion is limited in areas with high gradient magnitude and encouraged in smooth areas. Actually the first term is the constraint curvature motion. The second term can be viewed as a shock filter since it pushes the level-lines towards valleys of high gradient.

Total variation

Total variation denoising, also known as total variation regularization. It is based on the principle that signals with excessive and possibly spurious detail have high total variation, that is the integral of the absolute gradient of the signal is high. According to this principle, reducing the total variation of the signal subject to it being a close match to the original signal, removes unwanted detail whilst preserving important details such as edges. For this principle, Rudin [24] in 1992 proposed to minimise the Total Variation as follows:

$$E(L) = \int_{\Omega} | \bigtriangledown L| d\Omega \tag{3.5}$$

under suitable boundary conditions.

To minimise the Total Variation the variational derivative must to set to zero: $\delta E(L) = 0$, [14] with

$$\delta E = - \bigtriangledown \cdot (| \bigtriangledown L|^{-1} \bigtriangledown L)$$

A PDE converging to the minimum is obtained by taking a steepest decent evolution:

$$L_t = -\delta E(L)$$

To avoid convergence to trivial solutions in the energy-based evolutions, we go to add constraints. However, the image L is composed of a blurred original image f and additive noise n, $L = Af + n$, with A a blurring kernel, one can estimate

$$\int_{\Omega} I(L) dx = \int_{\Omega} (Af - L)^2 dx = \sigma^2$$

where σ is the variance of the noise. This additional information can be combined with Eq. (3.5) using a Lagrange multiplier λ, and the general model to reconstruct f now becomes

$$min(E(L) + \lambda I(L))$$

with corresponding steepest decent PDE

$$L_t = -\delta E(L) - \lambda \delta I(L),$$

hence the total variation evolution is

$$L_t = \bigtriangledown \cdot (|\bigtriangledown L|^{-1} \bigtriangledown L) - \lambda A^*(Af - L)$$

Special Co-Dimension 1 and 2 Structures

We have gone through the gauge coordinates, and how the local derivative form the the local coordinate system. At first, one clearly should consider the cases where these vanish. From Eqs. (3.1) and (3.2) it is clear that critical points L_{vv} and L_{ww} are undefined. In numerical cases this situation can be avoided by multiplying Eqs. (3.1) and (3.2) with L_w^2, although one then solves slightly different equations.

Moreover, unclear casses occur where a derivative can be defined in two different directions: ridges. Ridge occur when there is simply connected sequence of pixels having gray tone intensity values which are significantly higher (lower) in the sequence than those neighboring.

Critical points

We will show that critical points in the expressions L_{vv} and L_{ww} are undefined.

Assume the determinant of the Hessian is nonzero at these points, then a local environment can be found as

$$L = \frac{1}{2}ax^2 + \frac{1}{2}by^2$$

where $a, b \in \{1, -1\}$. For an extremum $ab = 1$, for a saddle $ab = -1$. Then, since $a^2 = b^2 = 1$

$$L_{vv} = \frac{bx^2 + ay^2}{x^2 + y^2},$$

$$L_{ww} = \frac{ax^2 + by^2}{x^2 + y^2},$$

we have then

$$\lim_{x \longrightarrow 0} l_{ww} = b = L_{yy},$$

$$\lim_{y \longrightarrow 0} l_{ww} = a = L_{xx},$$

$$\lim_{x \longrightarrow 0} l_{vv} = a = L_{xx},$$

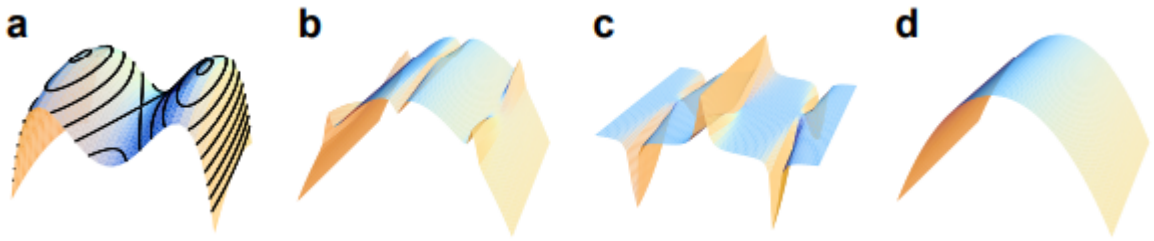

Figure 3.4: Ridge behaviour of Eq.(3.6) . From left to right: (a) The intensity L as function of x and y, with several isophotes. (b) L_{ww} on the same (x,y) domain. (c) L_{vv} on the same (x, y) domain. (d) $L_{ww} + L_{vv}$ on the same (x, y) domain [12].

$$\lim_{y \longrightarrow 0} l_{vv} = b = L_{yy},$$

The values converge to the same value around each exterma, and do not converges at the saddle points where $a = -b$. The saddle point may change its position. because of the change of the local environment.

Note that L_t is positive (negative) at a minimum (maximum). Hence, extrema are not enhanced and structure will vanish, through the evolution.

Note: In many applications, these casses do not happen, since numerically at least one will not have a critical points and obtain non-zero values for the derivatives.

Ridges

In this section we will cosider an arbitrary expression that shows the behaviour at ridges,

$$L = -x^4 + 2a^2x^2 - \epsilon y^2, \quad -1 \ll \epsilon < 0 \tag{3.6}$$

Now we will rewrite Eqs. (3.1) and (3.2), note that $L_{xy} = 0$, and therefore the second-order gauge derivatives of L are as follows:

$$L_{vv} = L_{xx} + L_x^2 \frac{L_{yy} - L_{xx}}{L_x^2 + L_y^2},$$

$$L_{ww} = L_{xx} + L_y^2 \frac{L_{yy} - L_{xx}}{L_x^2 + L_y^2}.$$

Therefore,

$$L_{vv} + L_{ww} = -12x^2 + 4a^2 - 2\epsilon$$

The ridges are formed by the curves when $x = 0$ and $x = \pm a$. Critical points occur at $(x, y) = \{(0, 0), (\pm a, 0)\}$ see also Fig. (3.4.a) .

For $L_x, L_y \neq (0,0)$, we have that $L_y^2 = O(\epsilon^2)$ and $L_{yy} = O(\epsilon)$, so $L_{vv} \approx 0$, and $L_{ww} \approx L_{xx}$

For $L_x = 0$, $L_{ww} = L_{yy} \approx 0$ and $L_{vv} = L_{xx}$. The latter equals $4a^2$ if $x = 0$ and $-8a^2$ if $x = \pm a$.

Thus L_{vv} is flat except for a small environment of the ridges, where peaks occur, see Fig. (3.4c). Where the Height of the ridges are come down, and the valley of the ridges are dragged up.

The evolution by L_{ww} will smear out everywhere, while the effect is smallest in the area close to the ridges: $L_{ww} = 0$ implies

$$L_x^2 L_{xx} = -L_y^2 L_{yy}, \quad i.e.\ L_x^2 L_{xx} = 8\epsilon^3 y^2 \approx 0,$$

see Fig. (3.4b). This is obvious, as it is the complement of Gaussian blurring with respect to L_{vv} : it corrects the deviation of the smooth surface

$$L_{xx} + L_{yy} = -12x^2 + 4a^2 - 2\epsilon$$

that is caused by L_{vv}, see Fig. (3.4d) .

Geometric PDEs: Second Order Gauge Derivatives

For large values of p, the p-Laplacian affected significantly by the term L_w^{p-2}. Hence, the two different expressions for the second-order derivatives in gauge coordinates, Eqs. (3.1) and (3.2) can be combined linearly in a PDE setting. Consequently, potential interesting flows are given by

$$L_t = pL_{vv} + qL_{ww}, \qquad p, q \in \mathbb{R} \tag{3.7}$$

with $L(t = 0) = L_0$.

Clearly, by setting $p \neq 0$ one can rescale t by $tf(p)$ and obtain, with $r = \dfrac{q}{p}$, the one parameter driven equation

$$L_t = L_{vv} + rL_{ww}, \qquad r \in \mathbb{R}. \tag{3.8}$$

Similarly we obtain a similar equation by setting $q \neq 0$, Note that Eq. (3.8) expresses an often desired ability to steer Mean Curvature Motion flow ($r = 0$) .

A General Solution: Qualitative Behavior

In this section we derive the general solution for Eq. (3.7). As is the case with gauge coordinates, it is assumed that the solution is independent of direction, size, dimension, and orientation. Therefore the dimensionless variable $\xi = \frac{x^2+y^2}{t}$ is used. Second, an additional t-dependency is assumed. This is inspired by the observation that the solution for $p = q = 1$ (the Gaussian filter) contain the factor t^{-1}.

The case $q \neq 0$

the starting assumption reads

$$L(x, y; t) = t^n f(\xi).$$

Then Eq. (3.7) is expressed as

$$t^{n-1}(-nf(\xi) + (2(p+q)+\xi)f'(\xi) + 4q\xi f''(\xi)) = 0.$$

To get this equation notice that

$$L_x = 2t^{n-1}xf'(\xi),$$

$$L_y = 2t^{n-1}yf'(\xi),$$

$$L_{xx} = 2t^{n-1}f'(\xi) + 4t^{n-1}\frac{x^2}{t}f''(\xi),$$

$$L_{yy} = 2t^{n-1}f'(\xi) + 4t^{n-1}\frac{y^2}{t}f''(\xi),$$

$$L_x^2 L_{yy} = 4t^{2n-2}x^2(f'(\xi))^2 \cdot \left(2t^{n-1}f'(\xi) + 4t^{n-1}\frac{y^2}{t}f''(\xi)\right),$$

$$L_y^2 L_{xx} = 4t^{2n-2}y^2(f'(\xi))^2 \cdot \left(2t^{n-1}f'(\xi) + 4t^{n-1}\frac{x^2}{t}f''(\xi)\right),$$

$$L_x^2 L_{xx} = 4t^{2n-2}x^2(f'(\xi))^2 \cdot \left(2t^{n-1}f'(\xi) + 4t^{n-1}\frac{x^2}{t}f''(\xi)\right),$$

$$L_y^2 L_{yy} = 4t^{2n-2}y^2(f'(\xi))^2 \cdot \left(2t^{n-1}f'(\xi) + 4t^{n-1}\frac{y^2}{t}f''(\xi)\right),$$

$$L_{xy} = 4t^{n-1}\frac{xy}{t}f''(\xi),$$

$$2L_x L_y L_{xy} = 32t^{3n-4}x^2y^2(f'(\xi))^2 f''(\xi),$$

$$L_x^2 + L_y^2 = 4t^{2n-1}(f'(\xi))^2\xi,$$

$$L_x^2 L_{yy} + L_y^2 L_{xx} - 2L_x L_y L_{xy} = 8t^{3n-2}(f'(\xi))^3\xi,$$
$$L_x^2 L_{xx} + L_y^2 L_{yy} + 2L_x L_y L_{xy} = 8t^{3n-2}(f'(\xi))^3\xi + 16t^{3n-2}(f'(\xi))^2 f''\xi^2$$

Using Eqs .(3.1) and (3.2)

$$\begin{aligned} L_{vv} &= \frac{L_x^2 L_{yy} + L_y^2 L_{xx} - 2L_x L_y L_{xy}}{L_x^2 + L_y^2} \\ &= \frac{8t^{3n-2}(f'(\xi))^3\xi}{4t^{2n-1}(f'(\xi))^2\xi} \\ &= 2t^{n-1}f'(\xi), \end{aligned}$$

$$\begin{aligned} L_{ww} &= \frac{L_x^2 L_{xx} + L_y^2 L_{yy} + 2L_x L_y L_{xy}}{L_x^2 + L_y^2} \\ &= \frac{= 8t^{3n-2}(f'(\xi))^3\xi + 16t^{3n-2}(f'(\xi))^2 f''\xi^2}{4t^{2n-1}(f'(\xi))^2\xi} \\ &= = 2t^{n-1}f'(\xi) + 4t^{n-1}f''(\xi)\xi. \end{aligned}$$

Hence,

$$L_t = nt^{n-1}f(\xi) + t^n f'(\xi)\cdot -\frac{x^2+y^2}{t^2} = t^{n-1}\left(nf(\xi) - f'(\xi)\xi\right).$$

Therefore Eq. (3.7)

$$L_t = pL_{vv} + qL_{ww}$$

leads

$$t^{n-1}\left(-nf(\xi) + f'(\xi)\xi + 2pf'(\xi) + 2qf'(\xi) + 4qf''(\xi)\xi\right) = 0$$

or

$$t^{n-1}(-nf(\xi) + (2(p+q)+\xi)f'(\xi) + 4q\xi f''(\xi)) = 0.$$

The solution of this ODE with respect to $f(\xi)$ and ξ is given by

$$f(\xi) = e^{-\frac{\xi}{4q}}\left(c_1 U\left(n + \frac{p+q}{2q}, \frac{p+q}{2q}, \frac{\xi}{4q}\right) + c_2 L^{\frac{p-q}{2q}}_{-\frac{p+2nq+q}{2q}}\left(\frac{\xi}{4q}\right)\right)$$

Here $U(a,b,z)$ is a confluent hypergeometric function and $L_a^b(z)$ is the generalised Laguerre polynomial expression . Taking $r = \dfrac{p+q}{2q}$, we find

$$L(x,y;t) = e^{-\frac{x^2+y^2}{4qt}} t^n \left(c_1 U\left(n+r, r, \frac{x^2+y^2}{4qt}\right) + c_2 L_{-n-r}^{r-1}\left(\frac{x^2+y^2}{4qt}\right)\right). \quad (3.9)$$

As we are working with images intensities, we need positive values . This is obtained by setting $n = -r$. Then the formula reduces for $n = -r$, since $U(0,.,.) = L_0(.) = 1$. Then the part between brackets in Eq. (3.9) reduces to $(c_1 + c_2)$, which is evaluates to be $\dfrac{1}{4\pi q}$. Thus This gives the following positive solutions of Eq.(3.7)

$$L(x,y;t) = \frac{t^{-\frac{p+q}{2q}}}{4\pi q} e^{-\frac{x^2+y^2}{4qt}}$$

The simplified diffusion $(p,q) = (b-1,1)$

$$L_t = L_{ww} + (b-1)L_{vv}$$

has solution

$$L(x,y;t,b) = \frac{1}{4\pi t^{b/2}} e^{\frac{-x^2-y^2}{4t}}.$$

For $b = 2$ the filter is linear, resulting in the Gaussian filter $(p = q = 1)$

$$L_t = L_{ww} + L_{vv} = \triangle L.$$

For $b = 1$ one obtains maximal blurring

$$L_t = L_{ww}.$$

Note that a solution can only be obtained when $q = 0$. This implies that the direction L_{ww} (i.e. blurring) must be present in the flow.

The case $q = 0$. In the previous case, we have the requirement $q \neq 0$. To examine the case $q = 0$, a second assumption, the t dependency is included as a factor $g(t)$. So to find a solution for $L_t = L_{vv}$, with again $t \propto (x^2 + y^2)$, consider

$$L(x,y;t) = f\left(-\frac{x^2+y^2}{t}\right) g(t).$$

The function $f(x,y;t)$ is dimensionless and rotational invariant, since if

$$x' = xcos\theta - ysine\theta$$

$$y' = xsin\theta + ycos\theta$$

then

$$x^2 + y^2 = x'^2 + y'^2$$

and hence

$$f(-\frac{x^2+y^2}{t}) = (-\frac{x'^2+y'^2}{t}).$$

Then f, g need to satisfy

$$\frac{(x^2+y^2+2t)f'\left(-\frac{x^2+y^2}{t}\right)}{tf\left(-\frac{x^2+y^2}{t}\right)} + \frac{tg'^{(t)}}{g(t)} = 0 \tag{3.10}$$

The justification of Eq. (3.10) is as follows

$$L_x = f'\left(-\frac{x^2+y^2}{t}\right)g(t)\cdot -\frac{2x}{t},$$

$$L_x = f'\left(-\frac{x^2+y^2}{t}\right)g(t)\cdot -\frac{2y}{t},$$

$$L_x^2 = f'^2\left(-\frac{x^2+y^2}{t}\right)g^2(t)\cdot \frac{4x^2}{t^2},$$

$$L_x^2 = f'^2\left(-\frac{x^2+y^2}{t}\right)g^2(t)\cdot \frac{4y^2}{t^2},$$

$$L_{xx} = f''\left(-\frac{x^2+y^2}{t}\right)g(t)\cdot \frac{4x^2}{t^2} + f'\left(-\frac{x^2+y^2}{t}\right)g(t)\cdot \frac{-2}{t},$$

$$L_{yy} = f''\left(-\frac{x^2+y^2}{t}\right)g(t)\cdot \frac{4y^2}{t^2} + f'\left(-\frac{x^2+y^2}{t}\right)g(t)\cdot \frac{-2}{t},$$

$$L_x^2L_{yy} = f'^2\left(-\frac{x^2+y^2}{t}\right)f''\left(-\frac{x^2+y^2}{t}\right)g^3(t)\cdot\frac{16x^2y^2}{t^4} + f'^3\left(-\frac{x^2+y^2}{t}\right)g^3(t)\cdot\frac{-8x^2}{t^3},$$

$$L_y^2L_{xx} = f'^2\left(-\frac{x^2+y^2}{t}\right)f''\left(-\frac{x^2+y^2}{t}\right)g^3(t)\cdot\frac{16x^2y^2}{t^4} + f'^3\left(-\frac{x^2+y^2}{t}\right)g^3(t)\cdot\frac{-8y^2}{t^3},$$

$$L_xL_y = f'^2\left(-\frac{x^2+y^2}{t}\right)g^2(t)\cdot \frac{4xy}{t^2},$$

$$L_{xy} = f''\left(-\frac{x^2+y^2}{t}\right)g(t)\cdot \frac{4xy}{t^2},$$

$$2L_xL_yL_{xy} = f'^2\left(-\frac{x^2+y^2}{t}\right)f''\left(-\frac{x^2+y^2}{t}\right)g^3(t)\cdot\frac{32x^2y^2}{t^4}.$$

Using Eq. (3.1)

$$\begin{aligned} L_{vv} &= \frac{L_x^2L_{yy}+L_y^2L_{xx}-2L_xL_yL_{xy}}{L_x^2+L_y^2} \\ &= \frac{\frac{-8}{t^3}f'^3\left(-\frac{x^2+y^2}{t}\right)g^3(t)(x^2+y^2)}{\frac{4}{t^2}f'^2\left(-\frac{x^2+y^2}{t}\right)g^2(t)(x^2+y^2)} \\ &= \frac{-2}{t}f'\left(-\frac{x^2+y^2}{t}\right)g(t). \end{aligned}$$

Hence

$$L_t = f'\left(-\frac{x^2+y^2}{t}\right)\cdot\left(\frac{x^2+y^2}{t}\right)g(t)+f\left(-\frac{x^2+y^2}{t}\right)g'(t).$$

Since $L_t = L_{vv}$, then

$$\frac{-2}{t}f'\left(-\frac{x^2+y^2}{t}\right)g(t) = f'\left(-\frac{x^2+y^2}{t}\right)\cdot\left(\frac{x^2+y^2}{t}\right)g(t)+f\left(-\frac{x^2+y^2}{t}\right)g'(t)$$

$$\frac{1}{t^2}f'\left(-\frac{x^2+y^2}{t}\right)g(t)\left(x^2+y^2+2t\right)+f\left(-\frac{x^2+y^2}{t}\right)g'(t) = 0$$

divided by $tf\left(-\frac{x^2+y^2}{t}\right)g(t)$ to get

$$\frac{\frac{1}{t^2}f'\left(-\frac{x^2+y^2}{t}\right)(x^2+y^2+2t)}{tf\left(-\frac{x^2+y^2}{t}\right)}+\frac{g'^{(t)}}{tg(t)} = 0$$

or we write

$$\frac{(x^2+y^2+2t)f'\left(-\frac{x^2+y^2}{t}\right)}{tf\left(-\frac{x^2+y^2}{t}\right)}+\frac{tg'^{(t)}}{g(t)} = 0$$

Let $\xi = -\frac{x^2+y^2}{t}$ then $x = \sqrt{-y^2-t\xi}$. Thus Eq. (3.10) transformed into

$$\frac{(2-\xi)f'(\xi)}{f(\xi)} = -\frac{tg'(t)}{g(t)}.$$

Since sides depend on a different variable, they should equal a constant, Therefore, we get $(2-\xi)f'(\xi) = \alpha f(\xi)$ and $tg'(t) = -\alpha g(t)$ with the solutions $f(\xi) = (\xi - 2)^{-\alpha}c_1$ and $g(t) = t^{-\alpha}c_2$. Hence

$$L(x, y; t) = f(\xi)g(t) = (\xi t - 2t)^{-\alpha}c_1c_2 = C(x^2 + y^2 + 2t)^{-\alpha}$$

3.3 Numerical Implementation

The presence of noise in images is unavoidable. It may be introduced by the image formation process, image recording, image transmission, etc. These random distortions make it difficult to perform any required picture processing. Hence, to obtain a butter image enhancement we derive a constrained minimization algorithm as a time dependent nonlinear PDE, where the constraints are determined by the noise statistics.

Let the observed intensity function $L_0(x, y)$ denote the pixel values of a noisy image for $x, y \in \Omega$. Let $L(x, y)$ denote the desired clean image, so

$$L_0(x, y) = L(x, y) + n(x, y)$$

when n is the additive noise [24]. In our framework the constrained minimization problem is :

minimize

$$\int\int_{\Omega} \sqrt{L_x^2 + L_y^2}dxdy$$

subject to constraints involving the mean

$$\int\int_{\Omega} Ldxdy = \int\int_{\Omega} L_0dxdy$$

This constraint signifies the fact that the white noise $n(x, y)$ is of zero mean and

$$\int\int_{\Omega} \frac{1}{2}(L - L_0)^2dxdy = \sigma^2$$

where $\sigma > 0$

Thus, we optain the following:

$$min \int\int_{\Omega} \left(\sqrt{L_x^2 + L_y^2} + \lambda_1(L - L_0) + \lambda_2 \left(\frac{1}{2}(L - L_0)^2 - \sigma^2 \right) \right) dxdy.$$

The solution is obtained by the Euler Lagrange equation,

$$\delta E = F_L - \frac{\partial}{\partial x} F_{L_x} - \frac{\partial}{\partial y} F_{L_y} = 0$$

Hence,

$$-\frac{\partial}{\partial x}\left(\frac{L_x}{\sqrt{L_x^2 + L_y^2}}\right) - \frac{\partial}{\partial y}\left(\frac{L_y}{\sqrt{L_x^2 + L_y^2}}\right) + \lambda_1 + \lambda_2(L - L_0) = 0$$

in Ω, with $\frac{\partial L}{\partial n} = 0$ on the boundary of $\Omega, \partial\Omega$.

The solution procedure uses a parabolic equation with time as an evolution parameter, or equivalently, the gradient descent method. This means that we solve

$$L_t = \frac{\partial}{\partial x}\left(\frac{L_x}{\sqrt{L_x^2 + L_y^2}}\right) + \frac{\partial}{\partial y}\left(\frac{L_y}{\sqrt{L_x^2 + L_y^2}}\right) - \lambda(L - L_0)$$

for $t > 0, x, y \in \Omega$, $L(x, y, 0)$ given, $\frac{\partial L}{\partial n} = 0$ on $\partial\Omega$

As t increases, we approach a denoised version of our image. We must compute $\lambda(t)$. We merely multiply the equation by $(L - L_0)$ and integrate by parts over Ω. We then have

$$\lambda = -\frac{1}{2\sigma^2}\int_\Omega \left[\sqrt{L_x^2 + L_y^2} - \left(\frac{(L_0)_x L_x}{\sqrt{L_x^2 + L_y^2}} + \frac{(L_0)_y L_y}{\sqrt{L_x^2 + L_y^2}}\right)\right] dxdy$$

With $\delta I = L - L_0, \lambda = \frac{<\delta E, \delta I>}{<\delta I, \delta I>}$, and$< \delta I, \delta I >= 2\sigma^2$. When we set $\lambda = 0$, an unconstrained blurring process is obtained. Alternatively, λ can be regarded as a penalty parameter that limits the L^2 difference between the input and output images. A too small value will cause an evolution that forces the image to stay close to the input image

P-Laplacians

For numerical implementation, consider the diffusivity estimation

$$\triangle L = C D_{i,j}^- \left(\left|D_{i,j}^+ f\right|^{p-2} D_{i,j}^+ f\right) \tag{3.11}$$

at a pixel (i, j). we forward and backward Euler scheme to compute Eq. (3.11) i.e.

$$D_i^+ f = f(i+1, j) - f(i, j), \quad D_i^- f = -f(i-1, j) + f(i, j)$$

and

$$D_j^+ f = f(i, j+1) - f(i, j), \quad D_j^- f = -f(i, j-1) + f(i, j).$$

Figure 3.5: Original image and a close up showing artifacts at edges

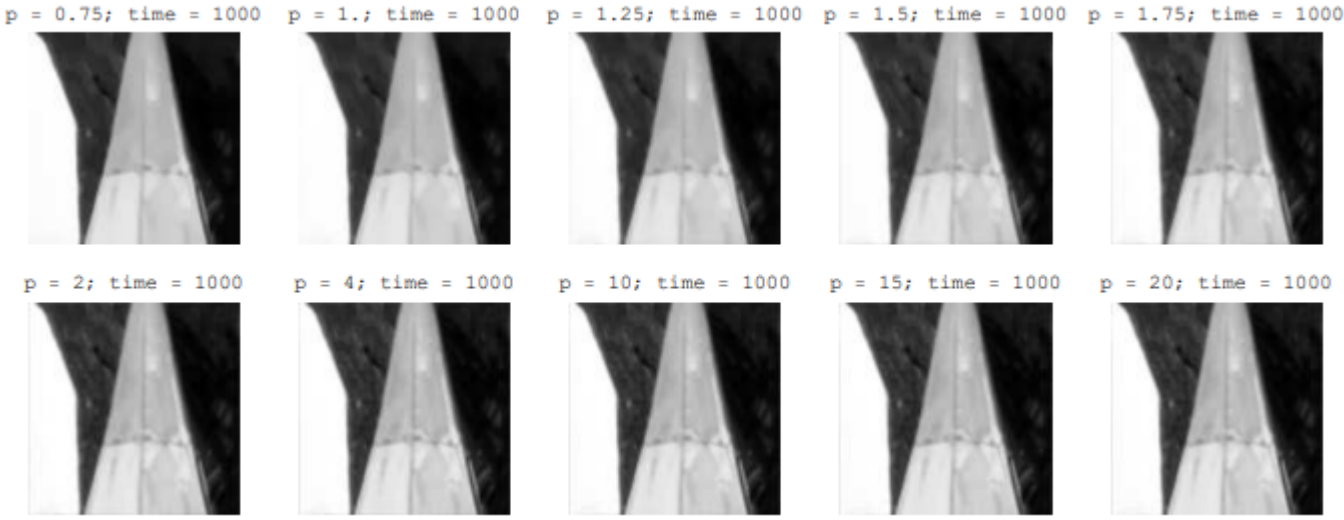

Figure 3.6: Constrained p-Laplacian evolution for several values of p [13]

To stabilise numerical computation for large p values, we choose the costnant C such that the maximum update is less or equal to 10 percent of the maximal image intensity . Values of $p \in \{0.75, 1, 1.25, 1.5, 1.75, 2, 4, , 10, 15, 20\}$, with 1000 iterations are computed. Note that p-Laplacians are defined for $1 < p < \infty$, but $p = 0.75$ - cartooning with extra deblurring - gives still stable results

Example 3.3.1 *Fig. (3.6) shows a convergence after approximately 400 iterations For the constrained evolution. However, For the unconstrained evolution convergence is obviously not obtained. Fig. (3.7) for large values of p, the p-Laplacian gets highly influenced by the gradient term. Hence, the updates are tempered. It seems that blurring is obtained without affecting the noise.*

Geometrical Evolution

The PDE is implemented using Gaussian derivatives $L_t = pL_{vv} + qL_{ww}$. As a

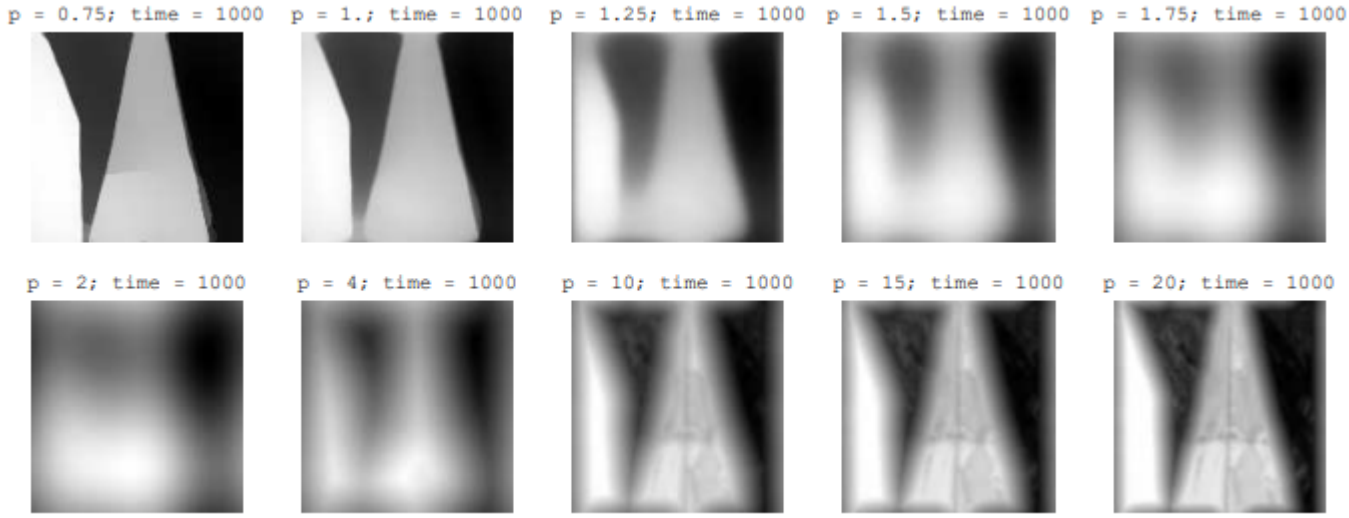

Figure 3.7: Unonstrained p-Laplacian evolution for several values of p [13].

consequence, larger time steps can be taken. When the spatial derivatives are computed as a convolution of the original image L with derivatives of a Gaussian G, the following results hold

$$\begin{aligned}(G * L)_x &= \left(\frac{1}{4\pi t} e^{\frac{-(x^2+y^2)}{4t}} * L\right)_x \\ &= \left(\frac{-2x}{4t} \cdot \frac{1}{4\pi t} e^{\frac{-(x^2+y^2)}{4t}}\right) * L \\ &= \left(\frac{-x}{2t} G\right) * L,\end{aligned}$$

$$\begin{aligned}(G * L)_{xx} &= \left(\frac{1}{4\pi t} e^{\frac{-(x^2+y^2)}{4t}} * L\right)_{xx} \\ &= \left(\frac{x^2}{(2t)^2} G + \frac{-1}{2t} G\right) * L \\ &= \left(\frac{x^2 - 2t}{4t^2} G\right) * L,\end{aligned}$$

$$
\begin{aligned}
(G * L)_{xy} &= \left(\frac{1}{4\pi t} e^{\frac{-(x^2+y^2)}{4t}} * L\right)_{xy} \\
&= \left(\frac{-x}{2t} \cdot \frac{-y}{2t} G\right) * L \\
&= \left(\frac{xy}{4t^2} G\right) * L,
\end{aligned}
$$

similarly we optain L_y and L_{yy}

$$(G * L)_y = \left(\frac{-y}{2t} G\right) * L,$$

$$(G * L)_{yy} = \left(\frac{y^2 - 2t}{4t^2} G\right) * L.$$

Consequently,

$$
\begin{aligned}
(G * L)_{xx} + (G * L)_{yy} &= \left(\frac{x^2 - 2t}{4t^2} G\right) * L + \left(\frac{y^2 - 2t}{4t^2} G\right) * L \\
&= \left(\frac{x^2 + y^2 - 4t}{4t^2} G\right) * L.
\end{aligned}
$$

Moreover, Using Eqs. (3.1) and (3.2) we optain

$$
\begin{aligned}
(G * L)_{vv} &= \left(\frac{\frac{x^2}{4t^2} \cdot \frac{y^2-2t}{4t^2} + \frac{y^2}{4t^2} \cdot \frac{x^2-2t}{4t^2} - \frac{2xy}{4t^2} \cdot \frac{xy}{4t^2}}{\frac{x^2}{4t^2} + \frac{y^2}{4t^2}} G\right) * L \\
&= \left(\frac{-1}{2t} G\right) * L,
\end{aligned}
$$

$$
\begin{aligned}
(G * L)_{ww} &= \left(\frac{\frac{x^2}{4t^2} \cdot \frac{x^2-2t}{4t^2} + \frac{y^2}{4t^2} \cdot \frac{y^2-2t}{4t^2} + \frac{2xy}{4t^2} \cdot \frac{xy}{4t^2}}{\frac{x^2}{4t^2} + \frac{y^2}{4t^2}} G\right) * L \\
&= \left(\frac{x^2 + y^2 - 4t}{4t^2} G\right) * L,
\end{aligned}
$$

Then we have

$$
\begin{aligned}
pL_{vv} + qL_{ww} &= \left(\frac{-p}{2t} G\right) * L + \left(\frac{(x^2 + y^2 - 4t)q}{4t^2} G\right) * L \\
&= \left(\frac{q(x^2 + y^2) - 2t(p + q)}{4t^2} G\right) * L,
\end{aligned}
$$

and Eq. (3.7) is numerically computed by

$$\frac{L_{j,k}^{n+1} - L_{j,k}^{n}}{\triangle t} = \left(\frac{q(x^2+y^2) - 2t(p+q)}{4t^2} G \right) * L_{j,k}^{n}$$

where $L_{j,k}^{n} = \xi^n e^{i(jx+ky)}$ is the vonneuman solution. The double integral, the right hand side of the previous equation

$$\int_\Omega \int_\Omega \frac{(q((\alpha-x)^2+(\beta-y)^2) - 2t(p+q))}{16\pi t^3} \xi^n e^{i(jx+ky) - \frac{(\alpha-x)^2+(\beta-y)^2}{4t}} d\alpha d\beta \quad (3.12)$$

evaluates to $-\frac{1}{2t}(p + q(2t(j^2+k^2)-1))\xi^n e^{-t(j^2+k^2)+i(xj+ky)}$ which equals

$$-\frac{e^{-t(j^2+k^2)}(p+q(2t(j^2+k^2)-1))}{2t} L_{j,k}^{n} = \Psi \cdot L_{j,k}^{n}$$

Consequently, Eq. (3.12) reduces to

$$\xi - 1 = \triangle t \cdot \Psi$$

For stability, it is required $|\xi| \leq 1$. The minimum for Ψ is obtained by

$$\partial_j \Psi = 0, \quad \partial_k \Psi = 0, \ i.e. \ \ t = \frac{-p+3q}{2q(j^2+k^2)}$$

yielding the value $\Psi_{min} = \frac{-q}{t} e^{\frac{p-3q}{2q}}$ q . For the maximum step size we find $\xi_{max} = \frac{2t}{q} e^{\frac{p-3q}{2q}}$

Obviously, as the implementation is based on the solution of the heat equation, so the maximum step size is limited by the case $p = q = 1$, i.e. $\xi_{max} \leq 2te$. So for the L_{ww} flow ($p = 0$; $q = 1$) the step size $2te^{\frac{3}{2}}$ would yield instabilities. Secondly, for L_{vv} flow ($p = 1; q = 0$), Ψ reduces to $-\frac{e^{-t(j^2+k^2)}p}{2t}$. The minimum is obtained at $(j,k) = (0,0)$. We therefore can assume $j^2 + k^2 \geq 1$. Then

$$\Psi_{min} = -\frac{1}{2t} e^{-t}$$

and the minimum step size is $4te^t$.

Example 3.3.2 *The two original shapes " a noisy disk and a noisy square" are shown in Fig. (3.8). At first, evolution obtained for L_{vv} and L_{ww} by applying 10 time steps in finite difference scheme, are shown in Fig. (3.9) we can notes the artifacts at the corners, due to the directional preference of the first-order derivatives in the term $L_x L_y L_{xy}$.*

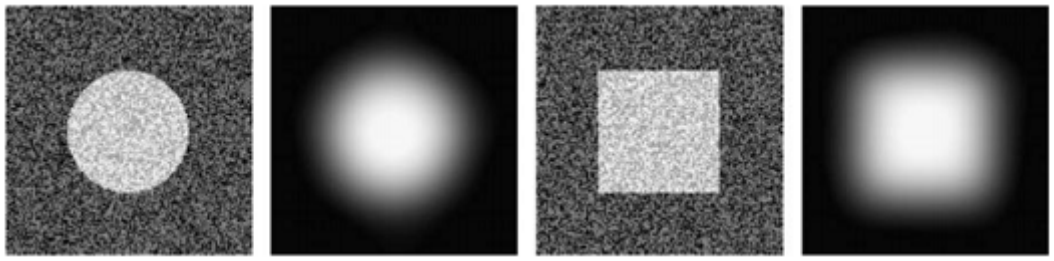

Figure 3.8: Disk and square with values $p = 0, q = 1$, with uniform random noise on (0, 1), and a Gaussian filter at $\sigma = \sqrt{128}$, [12].

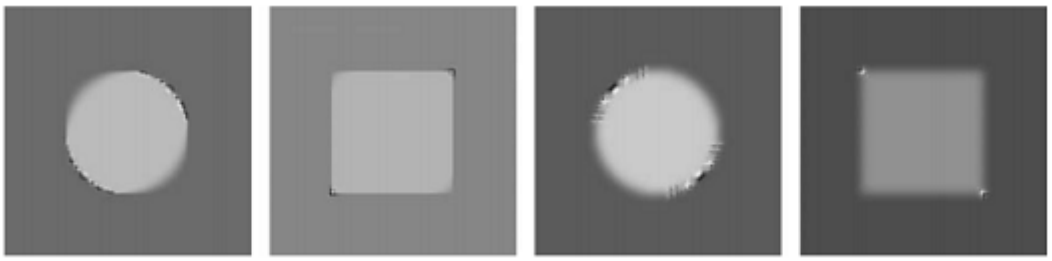

Figure 3.9: Evolution obtained for L_{vv} and L_{ww} by applying 10 time steps in finite difference scheme, at left the L_{vv} flow , and at right the L_{ww} flow for the noisy disk and square for these images [12].

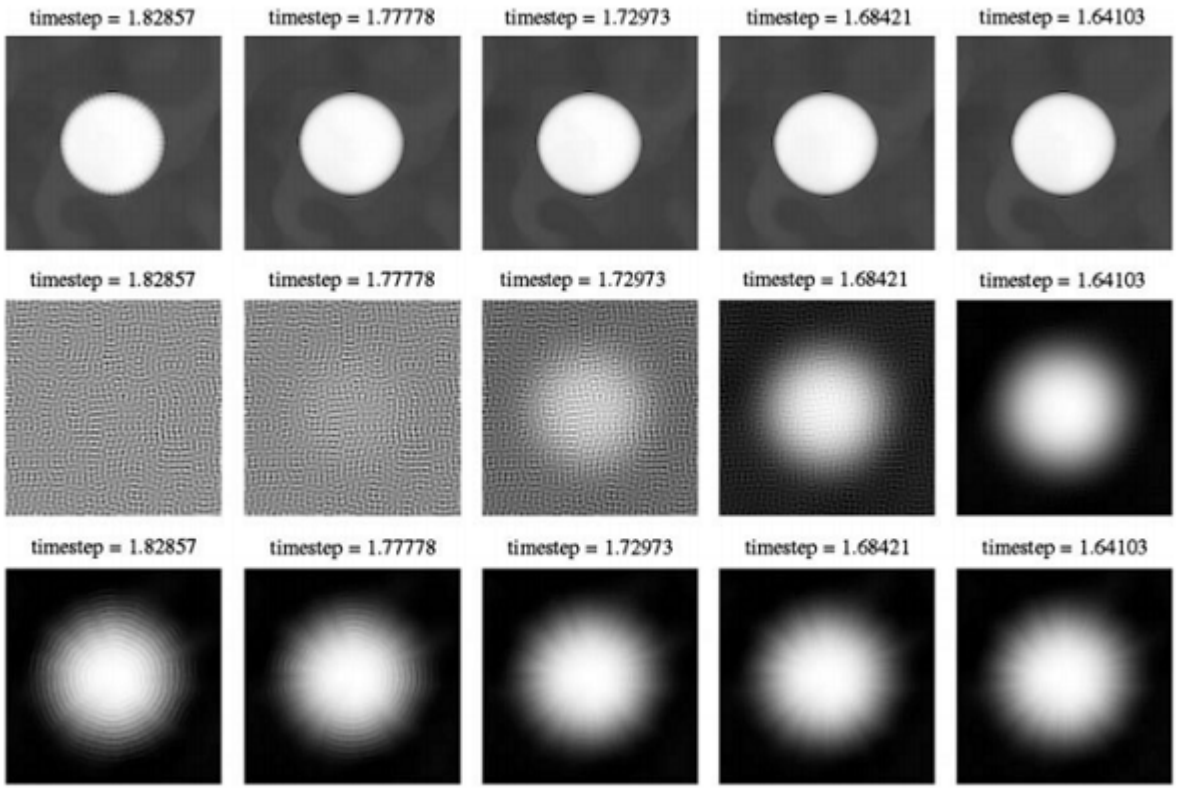

Figure 3.10: Results of the noisy disk , for Lvv flow (top row), Gaussian flow (middle row), and Lww flow (bottom row), for various time step ranges around the critical value $\triangle t = 2et = 2e\frac{1}{2}\sigma^2 = 1.74$, [12].

Example 3.3.3 *Figs. (3.10) and (3.11) shows the Gaussian derivatives implementation for the disk and square,in order to have a blurring of the original image with a Gaussian filter that equal to the linear evolution of the heat equation Gaussian flow, the total time t_t must be equal to* 64. *with $\sigma = \sqrt{2t_t} = \sqrt{128}$, Fig. (3.8). Since $64 = n \triangle t$, we let $n = 35, ..., 39$. The corresponding values for n are shown of top of each image.*

We tooke The scale of the derivative filters to be $\sigma = 0.8$, so the theoretical critical step size $\triangle t = 2et = 2e\frac{1}{2}\sigma^2 = 1.74$. One obviously sees the alteration around the critical values. Since comparatively much noise is added, the value is a bit lower that the predicted value. by taking a huge large time step, instability artifacts are apparent: For L_{vv} flow the results become peaky, while the L_{ww} flow shows ringing,it also show a very bad a Gaussian blurring .

Example 3.3.4 *The result of applying the Gaussian derivatives implementation of $L_t = pL_{vv} + qL_{ww}$ in 50 time steps is shown in Fig. (3.13). The evolution*

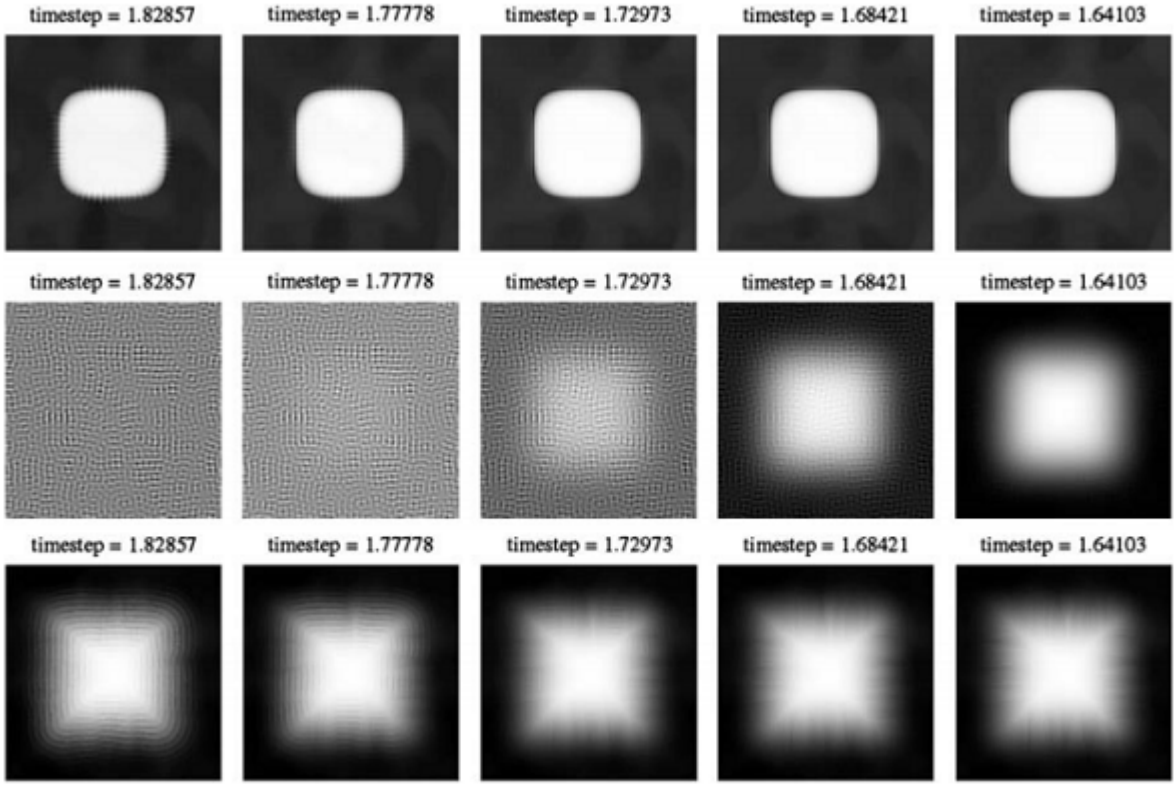

Figure 3.11: Results of the square for Lvv flow (top row), Gaussian flow (middle row), and Lww flow (bottom row), for various time step ranges around the critical value $\triangle t = 2et = 2e\frac{1}{2}\sigma^2 = 1.74$, [12].

Figure 3.12: Original image and a noisy one

shows the spiky artifacts for $p < 0$, while $q < 0$ shows the edges. The diagonal gives Gaussian (de)blurring. Moreover we get the pest result by appling $q = 0$.

3.4 The optimal homotopy asymptotic Method (OHAM)

In this section, we reformulate the the optimal homotopy asymptotic method (OHAM) for solving second order partial differential equation in gauge coordinates Eq. (3.7).

Basic Formulation of OHAM

Consider the operator equation of the form [16, 28]

$$A(L(x, y, t)) + f(x, y, t) = 0$$

where A is a differential operator, $L(x, y, t)$ is unknown function, and $f(x, y, t)$ a known analytic function. Assume further that A can be divided into two parts: M and N such that

$$A = M + N$$

where M is the simpler part of the partial differential equation which is easier to solve and N contains the remaining part of A. According to OHAM, one can construct an optimal homotopy map

$$L(x, y, t, r) : \Omega \times [0, 1] \longrightarrow \mathbb{R}$$

that satisfies the homotopy equation

$$(1 - r)[M(L(x, y, t, r)) + f(x, y, t)] - H(r)[A(L(x, y, t, r)) + f(x, y, t)] = 0, \quad (3.13)$$

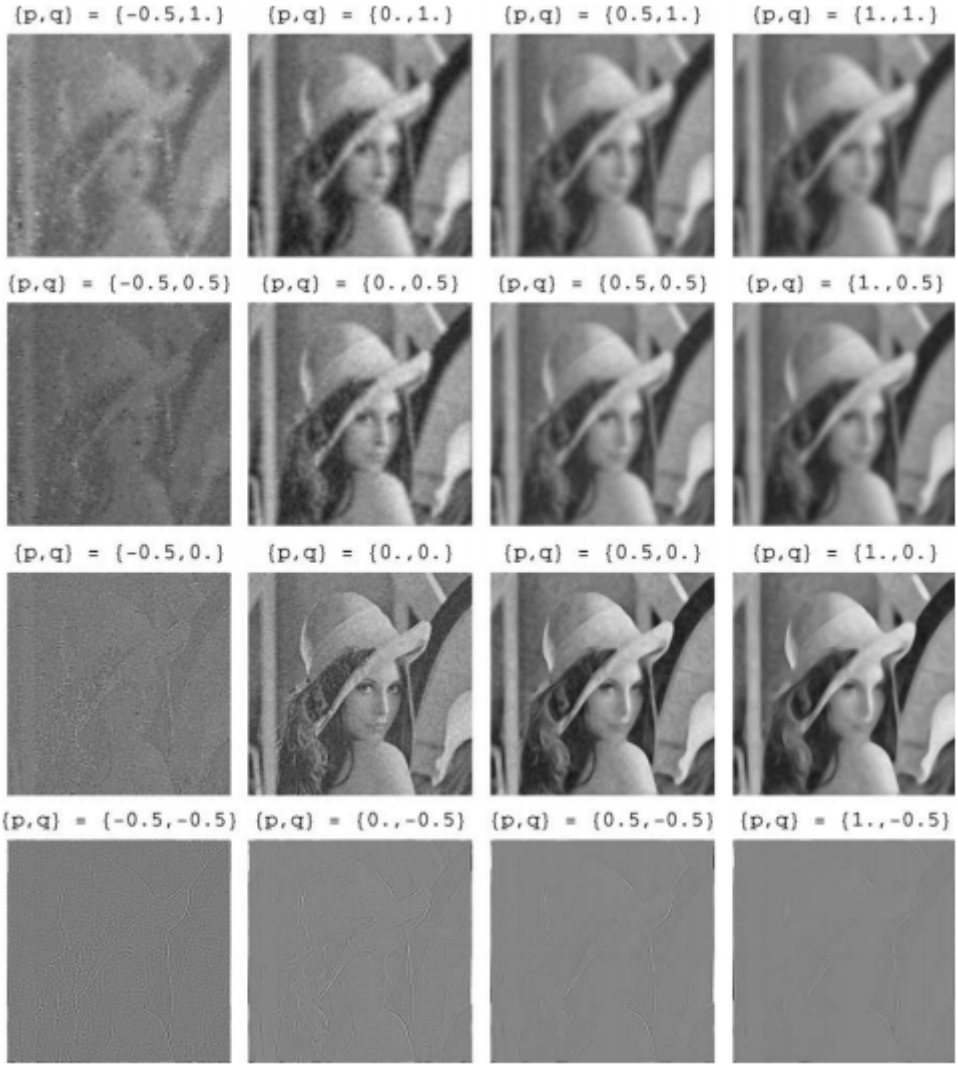

Figure 3.13: Geometrical evolution of $L_t = pL_{vv} + qL_{ww}$ for several values of p and q. There is no constraint. For negative p there are spiky artifacts, for positive ones there is blurring. For negative q one sees the edges [12].

$H(r)$ is auxiliary function such that $H(r) \neq 0$ for $r \neq 0$, $H(0) = 0$ and $r \in [0.1]$ is an embedding paramete.

From Eq.(3.13), if $r = 0$, we get $M(L(x, y, t, 0)) + f(x, y, t) = 0$, with solution $L(x, y, t, 0) = L_0(x, y)$,

and if $r = 1$, we get $M(L(x, y, t, 1)) + f(x, y, t) = 0$, with solution $L(x, y, t, 1) = L(x, y, t)$, i.e the exact solution.

Thus, as r varies from 0 to 1, the solution $L(x, y, t, r)$ arrives from $L_0(x, y)$ at $L(x, y, t)$. The auxiliary function H(r) is chosen of the form:

$$H(r) = \sum_{k=1}^{n} c_k r^k$$

where c_i, $i \in N$ are constants. To get an approximate solution, we expand $L(x, y, t, r, c_1, c_2, \dots)$ by Taylor's series, about r in the following manner:

$$L(x, y, t, r, c_1, c_2, \dots) = L_0(x, y, t) + \sum_{k=1}^{\infty} L_k(x, y, t, c_i) r^k \tag{3.14}$$

Substituting Eq. (3.14) into Eq. (3.13), and equating the coefficients of the like powers of r, we obtain the zeroth to the kth order problems governing equations of

$$L_0(x, y), L_1(x, y, t, c_i), \dots, L_k(x, y, t, c_i)$$

$$M(L_0(x, y, t)) + f(x, y, t) = 0,$$

$$M(L_1(x, y, t, c_i)) - M(L_0(x, y, t)) = c_1 N_0(L_0(x, y, t)),$$

$M(L_2(x, y, t, c_i)) - M(L_1(x, y, t, c_i)) = c_2 N_0(L_0(x, y, t)) + c_1(M(L_1(x, y, t, c_i))$
$+ N_1(L_0(x, y, t), L_1(x, y, t, c_i))),$

$M(L_k(x, y, t, c_i)) - M(L_{k-1}(x, y, t, c_i)) = c_k N_0(L_0(x, y, t))$
$+ \sum_{j=1}^{k-1} c_j(M(L_{k-1}(x, y, t, c_i)) + N_{k-1}(L_0(x, y, t), L_1(x, y, t, c_i), ..., y_{k-1}(x, y, t, c_i)),$

where $N_m(L_0(x, y, t), L_1(x, y, t, c_i), L_2(x, y, t, c_i), ..., L_m(x, y, t, c_i))$ is the coefficient of r^m in the expansion of $N(L(x, y, t; r, c_i))$ about the embeding parameter.

$$N(L(x, y, t, r, c_i)) = N_0(L_0(x, y)) + \sum_{k=1}^{\infty} N_k(L_k(x, y, c_i) r^k)$$

The convergence of the series in Eq. (3.14) is dependent upon the auxiliary constants $c_1, c_2, ...$ If it is convergent at $r = 1$, one has:

$$L(x, y, t, 1, c_i) = L_0(x, y) + \sum_{k=1}^{\infty} L_k(x, y, c_i)$$

This equation is the source of the required approximate solutions. Substituting from Eq. (3.14) into

$$M(L(x,y,t)) + N(L(x,y,t)) + f(x,y,t) = 0,$$

leads to the following residual formula

$$R(x,y,t,c_i) = M(L((x,y,t,c_i))) + N((x,y,t,c_i) + f(x,y,t)$$

If $R(x,y,t,c_i) = 0$, then $L(x,y,t,c_i)$ will be the exact solution. For the determination of auxiliary constant $c_i,\ i = 1,2,...,$ we apply the method of least squares:

$$J(c_i) = \int_\Omega \int_0^t R^2(x,y,s,c_i)dxdyds$$

where Ω is a subset of $\mathbb{R}^2$ depending on the given problem.

The unknown constants c_i can be identified from the conditions

$$\frac{\partial J}{\partial c_1} = \frac{\partial J}{\partial c_2} =, ..., = \frac{\partial J}{\partial c_m} = 0$$

With these constants known, the approximate solution is well-determined as

$$L^{(m)}(x,y,t) = L_0(x,y,t) + L_1(x,y,t,c_i) + L_2(x,y,t,c_i) + ... + L_m(x,y,t,c_i).$$

Application of OHAM to second order PDE with gauge coordinates .

Consider the second order gauge coordinates equation

$$L_t = pL_{vv} + qL_{ww}.$$

Applying OHAM as discussed above with

$$M = L_t, \quad N = -pL_{vv} - qL_{ww}$$

then Eq. (3.13) becomes

$$(1-r)(L_t) + H(r)(L_t - pL_{vv} - qL_{ww}) = 0 \tag{3.15}$$

Note that, by taking $r = 0$ in Eq. (3.15) we optain

$$L_t = 0$$

which leads to

$$L(x,y,t) = L_0(x,y)$$

and when we set $r = 1$, we get

$$L_t - pL_{vv} - qL_{ww} = 0$$

hence

$$L(x, y, t, 1) = L(x, y, t)$$

which is clearly, the exact solution that we are looking for. substituting from Eq. (3.14) in Eq. (3.15) we get

$$\begin{aligned}(1-r)\left(\frac{\partial}{\partial t}L_0(x,y,t) + \sum_{m=1}^{\infty}\frac{\partial}{\partial t}L_m(x,y,t,c_i)r^m\right) = H(r)\,(\,\frac{\partial}{\partial t}L_0(x,y,t) \\ + \sum_{m=1}^{\infty}\frac{\partial}{\partial t}L_m(x,y,t,c_i)r^m - p\frac{\partial^2}{\partial v^2}L_0(x,y,t) - \sum_{m=1}^{\infty}p\frac{\partial^2}{\partial v^2}L(x,y,t,c_i)r^m \\ - q\frac{\partial^2}{\partial w^2}L_0(x,y,t) - \sum_{m=1}^{\infty}q\frac{\partial^2}{\partial w^2}L(x,y,t,c_i)r^m\,)\,.\end{aligned} \tag{3.16}$$

Proceeding as before, with $H(r) = c_1 r$ we equate the coefficients of like powers of r in Eq. (3.16). Consequently, we get the following approximation.

The zeroth- order approximation. $L_0(x, y, t)$ satisfies

$$\frac{\partial}{\partial t}L_0(x,y,t) = 0, \quad L_0(x,y,0) = L_0(x,y). \tag{3.17}$$

The first order approximation, $L_1(x, y, t)$ satisfies

$$\frac{\partial}{\partial t}L_1(x,y,t,c_1) = -c_1 p\frac{\partial^2}{\partial v^2}L_0(x,y) - c_1 q\frac{\partial^2}{\partial w^2}L_0(x,y), \quad L_1(x,y,0,c_1) = 0. \tag{3.18}$$

The second order approximation, $L_2(x, y, t, c_1)$ satisfies

$$\frac{\partial}{\partial t}L_2(x,y,t,c_1) = (1+c_1)\frac{\partial}{\partial t}L_1(x,y,t,c_1) - c_1 p\frac{\partial^2}{\partial v^2}L_1(x,y,t,c_1) - c_1 q\frac{\partial^2}{\partial w^2}L_1(x,y,t,c_1), \tag{3.19}$$

$L_2(x, y, 0, c_1) = 0.$

The first order approximation can be rewritten using Eqs. (3.1) and (3.2) as follwos

$$L_1(x,y,t,c_1) = -c_1 tp\cdot\frac{(\frac{\partial L_0}{\partial x})^2\frac{\partial^2 L_0}{\partial y^2} + (\frac{\partial L_0}{\partial y})^2\frac{\partial^2 L_0}{\partial x^2} - 2\frac{\partial L_0}{\partial x}\frac{\partial L_0}{\partial y}\frac{\partial^2 L_0}{\partial x\partial y}}{(\frac{\partial L_0}{\partial x})^2 + (\frac{\partial L_0}{\partial y})^2}$$

$$- c_1 tq \cdot \frac{(\frac{\partial L_0}{\partial x})^2 \frac{\partial^2 L_0}{\partial x^2} + (\frac{\partial L_0}{\partial y})^2 \frac{\partial^2 L_0}{\partial y^2} + 2\frac{\partial L_0}{\partial x}\frac{\partial L_0}{\partial y}\frac{\partial^2 L_0}{\partial x \partial y}}{(\frac{\partial L_0}{\partial x})^2 + (\frac{\partial L_0}{\partial y})^2}$$

Note that, this approximation depends on the auxiliary constant c_1, finding it leads to the first overall order aproximation

$$L^{(1)}(x, y, t) = L_0(x, y) + L_1(x, y, t, c_1) \tag{3.20}$$

To determine c_1 we obtain the residual equation

$$R(x, c_1) = \frac{\partial}{\partial t}\left(L_0(x, y) + L_1(x, y, t, c_1)\right) - p\frac{\partial^2}{\partial v^2}\left(L_{.0}(x, y) + L_1(x, y, t, c_1)\right)$$
$$- q\frac{\partial^2}{\partial w^2}\left(L_0(x, y) + L_1(x, y, t, c_1)\right).$$

Hence we dedtermine c_1 such that

$$J(c_1) = \int_\Omega \int_0^t R^2(x, y, s)dxdyds \qquad \text{is minimum}$$

or we determine c_1 such that $\dfrac{\partial J}{\partial c_1} = 0$.

Now

$$\frac{\partial J}{\partial c_1} = \int_\Omega \int_0^t 2R(x, y, s)\frac{\partial R}{\partial c_1}dxdyds = 0$$

or

$$\frac{\partial J}{\partial c_1} = \int_\Omega \int_0^t R(x, y, s)\frac{\partial R}{\partial c_1}dxdyds = 0$$

which can be written as follows

$$\frac{\partial J}{\partial c_1} = \int_\Omega \int_0^t \left(-(1 + c_1) + c_1 t(p\partial^2_{v^2} + q\partial^2_{w^2})\right)(p\partial^2_{v^2} + q\partial^2_{w^2})L_0(x, y) \cdot \left(-1 + t(p\partial^2_{v^2} + q\partial^2_{w^2})\right)(p\partial^2_{v^2} + q\partial^2_{w^2})L_0(x, y)dxdyds = 0$$

We have then

$$c_1 = \frac{\int_\Omega \int_0^t (p\partial^2_{v^2} + q\partial^2_{w^2})L_0(x, y) \cdot \left(-1 + t(p\partial^2_{v^2} + q\partial^2_{w^2})\right)(p\partial^2_{v^2} + q\partial^2_{w^2})L_0(x, y)dxdyds}{\int_\Omega \int_0^t \left(\left(-1 + t(p\partial^2_{v^2} + q\partial^2_{w^2})\right)(p\partial^2_{v^2} + q\partial^2_{w^2})L_0(x, y)\right)^2 dxdyds} \tag{3.21}$$

Example

Let us consider the initial

$$L_0(x,y) = \begin{cases} x^3(x-2)^3y^3(y-2)^3, & \text{for } x,y \in [0,2] \\ 0, & \text{otherwise} \end{cases}$$

The exact solution [30] for the equation $L_t = \triangle L$ is

$$L(x,y,t) = \frac{1}{8\pi t}\int_0^2\int_0^2 e^{\frac{-(x-\xi)^2-(y-\eta)^2}{4t}}d\xi d\eta \tag{3.22}$$

for $x, y \in [0.2]$.

Taking $\Omega = [0,2]^2$ and $t \in [0,1]$. We apply a matlabe code to Eq. (3.21) to find the value of c_1 as follows,

for $p = 1$, $q = 0$, $c_1 = -0.1392$,

for $p = 0$, $q = 1$, $c_1 = -0.3192$,

and for $p = 1$, $q = 1$, $c_1 = 0.1892$.

The first order aproximation solution via OHAM Eq. (3.20)

$$\begin{aligned} L^{(1)}(x,y,t) &= L_0(x,y) + L_1(x,y,t,c_1) \\ &= x^3(x-2)^3y^3(y-2)^3 + -c_1t\left(p\frac{\partial^2}{\partial v^2}L_0(x,y) + q\frac{\partial^2}{\partial w^2}L_0(x,y)\right) \end{aligned}$$

Notice that for $p = 1$ and $q = 0$, at $x = 0.5,\ y = 0.5$ and $t = 0.5$,
$L^{(1)}(x,y,t) = -0.2008$,

for $p = 0$ and $q = 1$, at $x = 0.5,\ y = 0.5$ and $t = 0.5$, $L^{(1)}(x,y,t) = -0.1364$,

for $p = 1$ and $q = 1$, at $x = 0.5,\ y = 0.5$ and $t = 0.5$, $L^{(1)}(x,y,t) = 0.2440$.

And the exact solution, Eq. (3.22) can be approximated using simpson's rule to 0.2403

Conclusion

In the current work we discusse the use of operators that can be used to remove noise and enhance signal, and we evolve the main principles for designing noise reduction and signal enhancement filters in the frequency and time domains. We presented a line of approaches to evolve images that unify existing methods in a general framework, by a weighted combination of second order derivatives in terms of gauge coordinates. For the qualitative behaviour, a solution of the series was derived and its properties were briefly mentioned. Relations with anisotropic and general diffusion equations were given.Quantitative results were obtained by a novel implementation using Gaussian derivatives. The practical results are visualised on artificial images to study the method in detail, and on a real-life image showing the expected qualitative behaviour. Penalising the distance of the resulting output to the input image, one can vary the desired amount of blurring and denoising. The results were visualised and in accordance with the theoretical predictions. At the end of the thesis the optimal homotopy asymptotic method (OHAM) was applied to derive a solution to the second order Gauge coordinate equation, and an example were taken showing close approximation to the exact solution in the case $p = q = 1$.

Appendix

MATLAB Functions for the IIR filtring

$clearall;$
$moyenne = 0;$
$Fs = 200e3;$
$Ts = 1/Fs;$
$dt = 0 : Ts : 5e - 3 - Ts;$
$f1 = 1e3;$
$s = 5 * sin(2 * pi * f1 * dt)$
$ecart\_type = abs(s * .05)$
$noise = moyenne + ecart\_type. * randn(1, numel(s));$
$x = s + noise;$
$plot(x)$
$plot(x)$
$title('Noisysignal')$
$xlabel('Samples');$
$ylabel('Amplitude')$
$X\_mags = abs(fft(x));$
$figure(10)$
$plot(X\_mags)$
$xlabel('DFTBins')$
$ylabel('Magnitude')$
$num\_bins = length(X\_mags);$
$plot([0 : 1/(num\_bins/2 - 1) : 1], X\_mags(1 : num\_bins/2))$
$xlabel('Normalised\ frequency(\pi\ rads/sample)')$
$ylabel('Magnitude')$
$[b_1, a_1] = butter(1, a)$
$H = freqz(b_1, a_1, floor(num\_bins/2));$
$holdon$
$plot([0 : 1/(num\_bins/2 - 1) : 1], abs(H), 'r');$
$x_filtered = filter(b_1, a_1, x);$
$figure(2)$
$plot(x\_filtered, 'r')$
$title('Filtered\ Signal')$
$xlabel('Samples');$
$ylabel('Amplitude')$

References

[1] Musa Alrefaya and Hichem Sahli. "A novel adaptive probabilistic nonlinear denoising approach for enhancing PET data sinogram". In: *Journal of Applied Mathematics* 2013 (2013).

[2] MJJC Annegarn, AHHJ Nillesen, and JG Raven. "Digital signal processing in television receivers". In: *Philips technical review* 42.6-7 (1986), pp. 183–200.

[3] Gunnar Aronsson. "On the partial differential equation $u_x^2 u_{xx} + 2u_x u_y u_{xy} + u_y^2 u_{yy} = 0$". In: *Arkiv för matematik* 7.5 (1968), pp. 395–425.

[4] Gilles Aubert and Pierre Kornprobst. *Mathematical problems in image processing: partial differential equations and the calculus of variations*. Vol. 147. Springer Science & Business Media, 2006.

[5] Frédéric Cao. *Geometric curve evolution and image processing*. Springer Science & Business Media, 2003.

[6] Vicent Caselles, J-M Morel, and Catalina Sbert. "An axiomatic approach to image interpolation". In: *Proceedings of International Conference on Image Processing*. Vol. 3. IEEE. 1997, pp. 376–379.

[7] Stephan Didas and Joachim Weickert. "Combining curvature motion and edge-preserving denoising". In: *International Conference on Scale Space and Variational Methods in Computer Vision*. Springer. 2007, pp. 568–579.

[8] Bart M ter Haar Romeny et al. "Differential structure of images: Accuracy of representation". In: *Proceedings of 1st International Conference on Image Processing*. Vol. 1. IEEE. 1994, pp. 21–25.

[9] Anil K Jain. "Partial differential equations and finite-difference methods in image processing, part 1: Image representation". In: *Journal of optimization Theory and Applications* 23.1 (1977), pp. 65–91.

[10] Dr Kuldeep Kaur and Mandeep Singh Saini. "Design IIR Notch Filter and Comb Filter to Eliminate Unwanted Frequencies for Environment". In: *International Journal of Advanced Research in Computer Engineering & Technology (IJARCET)* 3.6 (2014).

[11] Jan J Koenderink. "The structure of images". In: *Biological cybernetics* 50.5 (1984), pp. 363–370.

[12] Arjan Kuijper. "Geometrical PDEs based on second-order derivatives of gauge coordinates in image processing". In: *Image and Vision Computing* 27.8 (2009), pp. 1023–1034.

[13] Arjan Kuijper. *Image processing with geometrical and variational pdes*. na, 2007.

[14] Arjan Kuijper. "The deep structure of Gaussian scale space images". PhD thesis. 2002.

[15] Tony Lindeberg. "Scale-space: A framework for handling image structures at multiple scales". In: (1996).

[16] Fazle Mabood. "The Application of Optimal Homotopy Asymptotic Method for One-Dimensional Heat and Advection-Diffusion Equations". In: *Inf. Sci. Lett* 2.2 (2013), pp. 57–61.

[17] Twan Maintz. "Digital and medical image processing". In: *Universiteit Utrecht* (2005).

[18] Alan V Oppenheim and George C Verghese. *Signals, systems and inference*. Pearson, 2015.

[19] SJ Orfanidis. "Introduction to signal processing, Sophocles J". In: *Orfanidis, Rutgers University* 13 (2010), p. 795.

[20] Pietro Perona and Jitendra Malik. "Scale-space and edge detection using anisotropic diffusion". In: *IEEE Transactions on pattern analysis and machine intelligence* 12.7 (1990), pp. 629–639.

[21] Alexander D Poularikas. *Transforms and applications handbook*. CRC press, 2010.

[22] Paolo Prandoni and Martin Vetterli. *Signal processing for communications*. Collection le savoir suisse, 2008.

[23] Bart M Haar Romeny. *Front-end vision and multi-scale image analysis: multi-scale computer vision theory and applications, written in mathematica*. Vol. 27. Springer Science & Business Media, 2008.

[24] Leonid I Rudin, Stanley Osher, and Emad Fatemi. "Nonlinear total variation based noise removal algorithms". In: *Physica D: nonlinear phenomena* 60.1-4 (1992), pp. 259–268.

[25] Guillermo Sapiro. *Geometric partial differential equations and image analysis*. Cambridge university press, 2006.

[26] Karthik Selvan, Akhil C Joy, and Jegan RR. "Denoising of Impulse Noise Corrupted Image using Modified Directional Weighted Median Filter Method and Contrast Enhancement". In: Feb. 2014.

[27] Monika Singh, Saroj Dogra, and Rajesh Mehra. "'IIR Filter Design and Analysis using Notch and Comb Filter'". In: *International Journal of Scientific Research Engineering & Technology (IJSRET) Volume* 2 (2013), pp. 358–361.

[28] H Ullah et al. "Approximate solution of two-dimensional nonlinear wave equation by optimal homotopy asymptotic method". In: *Mathematical Problems in Engineering* 2015 (2015).

[29] Joachim Weickert. *Anisotropic diffusion in image processing*. Vol. 1. Teubner Stuttgart, 1998.

[30] David Vernon Widder. *The heat equation*. Vol. 67. Academic Press, 1976.

[31] Maciek Wielgus. "Perona-Malik equation and its numerical properties". In: *arXiv preprint arXiv:1412.6291* (2014).

[32] Andrew P Witkin. "Scale-space filtering". In: *Readings in Computer Vision*. Elsevier, 1987, pp. 329–332.

حول تطبيق المعادلات التفاضلية الجزئية في معالجة الصور

إعداد: سرين وليد احمد نصر

إشراف: الدكتور يوسف حسين زحايقة

ملخص:

في هذه الأطروحة، أولاً تم تقديم شرحا موجزًا للمفاهيم الاساسية في أنظمة الإشارات والأنظمة الخطية الثابتة زمنيا، وأنظمة تحويل فوريه المتقطع مع بعض خصائصه. كما تم اشتقاق معادلة الالتفاف "convolution theorem "، التي تسمح لنا بإيجاد مخرج النظام الخطي الثابت زمنيا لأي إشارة مدخلة. بالإضافة الى ذلك، تم الحديث عن استخدام الفلاتر التي يمكن استخدامها في إزالة الضوضاء وتحسين الإشارة، وعرض المبادئ الرئيسية لتصميم فلاتر للحد من الضوضاء وتعزيز الإشارة في مجالات التردد والوقت. وتم تقديم تصميم فلتر الشق "notch filter" وفلتر المشط "comb filter" المستخدم في إزالة التداخل الدوري، وتعزيز الإشارات الدورية، وفصل مكونات النصوع والتلوين في أنظمة التلفاز الملون الرقمي.

ثانيا، في معالجة الصور، تم اشتقاق وربط معادلات لابلاس من حيث مفاهيم إحداثيات القياس. تم ايضا تقديم العديد من الطرق والاساليب المستخدمة في تنقية الصور وتحسينها استنادًا إلى المعادلات التفاضلية الجزئية. لذلك تم التعريف بالسلوك النوعي من خلال استخلاص حل لهذه المعادلات التفاضلية الجزئية وذكر خصائصها. ومناقشة بعض المفاهيم مثل حركة الانحناء الوسطي ومعادلة الانتشار لتنقية الصور مع الحفاظ على الحواف. علاوة على ذلك، تم تنفيذ

النتائج الكمية والعددية على صور من واقع الحياة، تظهر السلوك النوعي المقيد والغير المقيد، حيث يمكن للإنسان أن يلاحظ مقدار الوضوح وتقليل الضوضاء. و في نهاية الأطروحة ، استخدمنا الأسلوب المعروف (OHAM) لاشتقاق حل للمعادلة إحداثيات القياس من الدرجة الثانية.